

Towards global time distribution via satellite-based sources of entangled photonsStav Haldar,^{1,*} Ivan Agullo,¹ Anthony J. Brady,^{1,†} Antía Lamas-Linares,² W. Cyrus Proctor,² and James E. Troupe³¹*Department of Physics & Astronomy, Louisiana State University, Baton Rouge, Louisiana 70803, USA*²*Amazon Web Services (AWS), Austin, Texas 78758, USA*³*Xairos Systems, Inc., Denver, Colorado 80124, USA*

(Received 1 November 2022; accepted 9 January 2023; published 21 February 2023)

We propose a satellite-based scheme to perform clock synchronization between ground stations spread across the globe using quantum resources. We refer to this as a quantum clock synchronization (QCS) network. Through detailed numerical simulations, we assess the feasibility and capabilities of a near-term implementation of this scheme. We consider a small constellation of satellites equipped only with modest resources. These include quantum devices such as spontaneous parametric down conversion sources, avalanche photodetectors, and moderately stable on-board clocks such as chip-scale atomic clocks. In our simulations, the various performance parameters describing the hardware have been chosen such that they are either already commercially available or require only moderate advances. We conclude that with such a scheme, establishing a global network of ground-based clocks synchronized to subnanosecond level (up to a few picoseconds) of precision would be feasible. Such QCS satellite constellations would form the infrastructure for a future quantum network, able to serve as a globally accessible entanglement resource. At the same time, our clock synchronization protocol provides the subnanosecond level synchronization required for many quantum networking protocols, and thus can be seen as adding an extra layer of utility to quantum technologies in the space domain designed for other purposes.

DOI: [10.1103/PhysRevA.107.022615](https://doi.org/10.1103/PhysRevA.107.022615)**I. INTRODUCTION**

The ability to measure, hold, and distribute time at high precision determines the limits of our scientific explorations. From a technological point of view, precise time measurement and synchronization is an indispensable feature of communication and networking protocols, navigation and ranging, astronomical, geological and meteorological measurements, among others. The goal of this paper is to assess the feasibility and quantify the capabilities of a concrete protocol to synchronize clocks based on the distribution of entangled photons by a constellation of satellites orbiting the Earth. The synchronization method used is a two-way optical scheme that exploits the features of spontaneously down-converted photon pairs to provide high-security time transfer. The basics of this method were proposed and described in Refs. [1,2] and a proof-of-principle experimental demonstration has been performed for ground-based static clocks [3], achieving synchronization precision of 51 ps in 100 s (data acquisition time) with relatively low pair rates, of order 200 s^{-1} for rubidium clocks separated by up to 50 meters (also see Refs. [4–6] for more recent demonstrations). We call this method quantum clock synchronization (QCS) since it utilizes single-photon detection, the fundamentally random timing of the photon pair production, and, for added security, the polarization entanglement between the photon pairs.

Important questions arise when trying to extend this protocol to include satellites in relative motion with ground

stations. These questions are related to both propagation effects—such as atmospheric losses, refraction, background counts, beam spreading, relativistic effects, etc.—as well as questions related to network scale and connectivity—e.g., what the farthest points on Earth are that can be synced and how often the sync will occur for a concrete network. To answer these questions, we develop (building upon previous work by some of us [7]) a software infrastructure to simulate the evolution of a satellite network and compute the real-time quantum data communication rates between ground stations and satellites, from which we can quantify the capabilities of the network and study its optimization. We show that such a timing system is capable of providing higher timing accuracy than achievable with traditional global navigation satellite system (GNSS) such as the global positioning system (GPS) at a global scale with a modest amount of resources.

The QCS network we consider here could achieve subnanosecond to picosecond accuracy utilizing a constellation of nanosatellites carrying lower stability, but very low size weight and power (SWaP) atomic clocks, such as the chip scale atomic clock (CSAC) [8]. These satellite clocks are then regularly and securely synchronized via optical links to a small group of much more stable ground-based reference atomic clocks. Such an architecture will derive a direct benefit from state-of-the-art atomic clock technology without the requirement that these clocks be low SWaP and space qualified. In addition, the use of low-cost nanosatellites would allow for cost effective upgrades of the system and robustness against hostile action against the constellation. Even though in the present paper we use satellites as intermediaries to synchronize ground stations, we envision global synchronization between satellites themselves and with stable

*hstav1@lsu.edu

†Present address: Department of Electrical and Computer Engineering, University of Arizona, Tucson, Arizona 85721, USA.

ground-based clocks, forming a master clock to which interested clientele (smaller, less stable clocks) can have access to.

To put our paper in perspective, we now give a brief survey of the abilities and drawbacks of classical clock synchronization techniques in the context of providing a high-precision secure global time standard. State-of-the-art optical clocks can achieve a fractional frequency instability below 1×10^{-18} [9] as measured by the clock's Allan deviation (ADEV) integrated over a period of an hour [10]. Additionally, great leaps have also been made towards synchronizing such high-precision, high-stability clocks. Researchers have recently developed sophisticated two-way time-stamping methods using radio frequency pulses that have been optimized to achieve a synchronization precision of up to tens of picoseconds [11]. Although these methods require a high degree of computational overhead due to the required radio frequency propagation modeling and data processing, at the highest achievable precision, there are state-of-the-art research results with classical optics-based protocols using optical frequency combs that can provide subfemtosecond precision time transfer with a stability of tens of femtoseconds (over a period of several days) through a few kilometers of atmospheric turbulence [12,13]. Such coherent techniques, however, become extremely difficult to implement over long distances and in high loss settings [14]. On the other hand, time over internet protocols such as the network time protocol and the precision time protocol (PTP) have global coverage but can achieve synchronization only to a few milliseconds and tenths of a microsecond, respectively, over long periods of time [15]. More recently, the White Rabbit protocol (a refinement of PTP developed at CERN) has achieved subnanosecond time distribution over fiber networks over distances of hundreds of kilometers [16].

At the submicrosecond level of precision, much more readily available is the use of GPS signals which can be used to provide almost continuous synchronization with an error of tens of nanoseconds (<40 ns, 95% of the time) [17]. While originally developed by the U.S. Department of Defense for precision global navigation and positioning to support military applications, GPS has become a defacto global time standard. In fact, a study in 2017 stated that of the estimated \$1.4 trillion of economic benefits that GPS has generated since it was made available for civilian and commercial use in the 1980s, well over half are directly based on precision timing and synchronization [18]. The ubiquity of GPS time information has been an important factor in the explosion of applications and technologies that rely on such a global time standard, e.g., 5G telecommunication networks. However, there are well-known issues regarding the security of GPS, e.g., the relative ease of jamming and spoofing GPS timing signals. In addition, while the nominal performance of GPS is impressive, future technologies such as 6G+ communication and quantum networks will require clock synchronization better than provided by GPS or other GNSSs [19,20].

Beyond the performance of GPS and other GNSS, another drawback is the high cost of these systems. The satellites required are very costly, with their large size required so as to contain the highly stable atomic clocks needed to achieve the required degree of synchronization. GPS satellites are regularly synchronized to each other by updates from ground

stations. However, to maintain the system's specified time accuracy with sufficient holdover to bridge these updates, the GPS satellite atomic clocks require stability on the order of 10^{-14} to 10^{-15} in terms of frequency accuracy [21]. Given these constraints, in this paper we propose a QCS network with the purpose of complementing existing classical techniques such as the GPS in providing a more precise, robust, and secure global time standard.

This paper is organized as follows. Section II describes the protocol used to synchronize satellite and ground-station clocks and to determine the clock offset from the two-way time-stamp correlation functions. Section III discusses the necessity and advantages of using a satellite constellation for building a global QCS network. Section IV gives a detailed account of our numerical simulations to estimate the performance of QCS networks and also provides a concrete example in the form of the QCS network servicing the continental U.S. at a subnanosecond time sync precision. In Sec. V, we summarize the key takeaways from our simulations. We then move on to Sec. VI that collects the main conclusions, discusses some shortcomings of the techniques used in this paper, and also proposes directions for future explorations.

II. QUANTUM CLOCK SYNCHRONIZATION PROTOCOL

This paper is primarily related to the question of time transfer or estimating the *time offset* between two separate clocks. We use the term QCS to describe the process of the exchange of quantum signals to estimate the time offset between remote clocks (see Refs. [1,22–27] for pioneering ideas on this field). The QCS protocol is a type of optical two way time and frequency transfer (O-TWTFT) scheme. Recall that a general O-TWTFT method uses signals transmitted symmetrically in both directions between Alice's and Bob's clocks to estimate the relative clock offset and frequency difference (sometimes referred to as frequency skew) between them. The central component of the clock offset estimation is the calculation of the cross correlations between the local time stamps of the photons produced by Alice and those received by Bob, and vice versa, out of which one can obtain the clock offset, as we explain below.

In the case of the QCS protocol, the classical optical signals are replaced with pairs of individual photons created via spontaneous down-conversion (SPDC) by pumping a nonlinear optical crystal. Due to conservation of energy, the time of birth of the photons are very highly correlated with each other, typically on the order of 10–100 fs [25,28]. In addition, the SPDC pair production process is quantum mechanically random with photon pair production following a Poisson distribution. The photon pair production time is itself used as the random code to be shared between Alice and Bob (truly random as opposed to pseudorandom in the classical case). Alice and Bob each have a SPDC source and locally detect one photon of each pair produced, recording a time stamp of each detection. The other photon from each down-converted pair is then transmitted to the other party and its detection is time stamped. The clock offset is then estimated by the difference of the two cross-correlation peaks as with the classical O-TWTFT scheme.

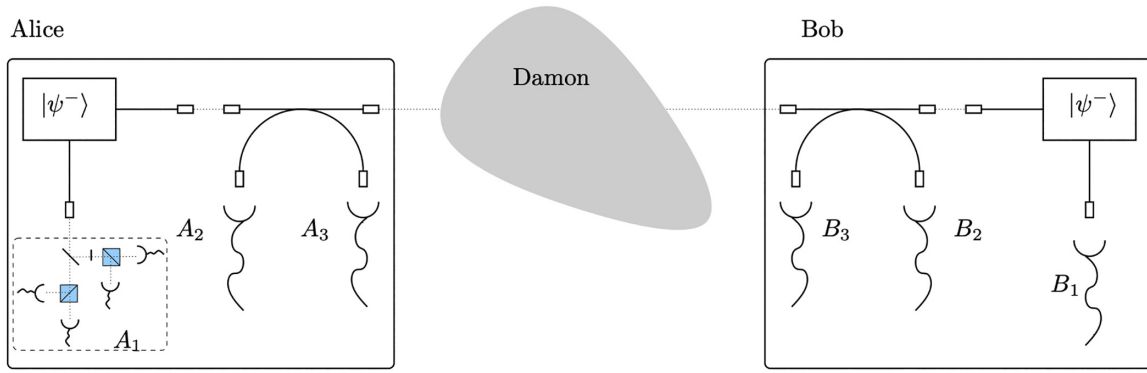


FIG. 1. Schematic for experimental implementation of the QCS protocol using entangled photons (details of this example setup are not important for the following discussion and are included for completeness). Alice and Bob each have a source of polarization entangled pairs ($|\psi^-\rangle$) produced by spontaneous parametric down-conversion (SPDC) and a set of single photon detectors within their secure laboratory (denoted by a solid line). Each mode of propagation of the photons ends in a detector cluster able to perform polarization measurements but only the cluster labeled as A_1 is fully represented in the figure. One member of the SPDC pair is detected locally at detector cluster A_1 on Alice's side (cluster B_1 on Bob's side). The other member of the pair is sent into a single mode fiber and propagated through a channel controlled by an adversary, Damon. Each of the propagating photons has a chance of being detected on the remote side by B_2 (A_2) for pairs originating at Alice's (Bob's) side. Times of arrival for all detected photons are recorded in each laboratory with respect to a local clock. Detectors A_3 and B_3 are under the control of either Alice or Bob and are included for completeness but do not play a part in the discussion. The detector cluster illustrated for A_1 represents a possible passive measurement scheme for a CHSH inequality. It uses a beam splitter followed by two polarizing beam splitters oriented at the appropriate angles for projection into the desired polarization state.

A. Clock offset estimate

Here we summarize the QCS protocol, as reported in Ref. [2] and with an experimental demonstration by Lee *et al.* [3] (See Fig. 1.) The reader is referred to these references and Ref. [1] for details omitted here. Following Ho *et al.* [1], we denote the numbers measured by Alice's (Bob's) local clock by t (t') with a subscript denoting a particular indexed event. If Alice and Bob were at the same spatial location detecting the same pair event, the difference between the times of detection as measured by their local clocks would be $\delta = t - t'$, and this δ would be the time offset that we aim to determine. If Alice and Bob are at separate locations, the time of propagation of a signal between Alice and Bob is denoted as Δt_{AB} (Δt_{BA} for propagation in the opposite direction). The round-trip time of a signal originating from either Alice or Bob is $\Delta T = \Delta t_{AB} + \Delta t_{BA}$.

To calculate the absolute time difference between clocks, δ , consider a photon pair produced at Alice's site. One of the members of the pair is detected locally at detector¹ A_1 and the other member of the pair travels to Bob accumulating a travel time Δt_{AB} and getting detected at B_2 . For any particular photon pair event produced at Alice's site, the difference between the time labels recorded at Alice and Bob will be

$$t' - t = \Delta t_{AB} + \delta.$$

Similarly, for any photon pair produced at Bob's site:

$$t - t' = \Delta t_{BA} - \delta.$$

¹Alice has two detectors, A_1 and A_2 , one dedicated to measure photons produced locally by Alice and the other to detect photons received from Bob. The same is true for Bob.

The differences between the time labels can be extracted by calculating a cross correlation between events at both sides. Consider first events produced at Alice's site. The detection events are translated into a distribution as

$$a(t) = \sum_i \delta(t - t_i) dt, \quad b(t') = \sum_j \delta(t' - t'_j) dt',$$

where i and j index arbitrary detection events which can arise either from the production of entangled pairs of photons or from other detector triggers such as stray light, dark counts, etc. The cross correlation is computed as

$$c_{AB}(\tau) = (a \star b)(\tau) = \int a(t)b(t + \tau) dt,$$

and, for sufficiently high signal-to-noise (SNR) ratio, will have a maximum at $\tau = \tau_{AB} = \Delta t_{AB} + \delta$. Likewise, if we consider those pairs created on Bob's site, we can extract another cross correlation,

$$c_{BA}(\tau) = (b \star a)(\tau) = \int b(t)a(t + \tau) dt,$$

which will have a maximum at $\tau = \tau_{BA} = \Delta t_{BA} - \delta$. Assuming channel reciprocity, i.e., $\Delta t_{AB} = \Delta t_{BA} = \Delta t$, from the above equations we can extract both the round-trip time (ΔT) and the absolute time difference between clocks without knowledge of the path length between Alice and Bob:

$$\Delta T = \tau_{AB} + \tau_{BA}, \quad \delta = \frac{1}{2}(\tau_{AB} - \tau_{BA}).$$

From this, we can see that the accuracy of the clock offset estimate is determined by the accuracy of estimates for each of the cross-correlation peaks.

Note that the quantum entanglement of photon pairs created at Alice's and/or Bob's locations does not play a direct role in determining the clock offset estimate, except that the

production of entangled pairs by SPDC ensures that the photons in each pair are generated within a time window typically of a few 100 fs—several orders of magnitude smaller than the timescales involved in the synchronization protocol. However, the entanglement between photon pairs can be used to increase the security of this protocol to malicious attacks.

Notice also that the protocols rest on the assumption of reciprocity in the time travel of light from Alice to Bob. In the case of free-space optical channels through the atmosphere, only very small deviations from full reciprocity are typically incurred. For instance, between a medium earth orbiting (MEO) satellite and ground station, the maximum error due to turbulence-induced nonreciprocity is predicted to be less than 10 fs [29,30]. Partial reciprocity and other nonidealities of practical implementations would likely place a limit on the achievable *secure* accuracy of the clock synchronization protocol.

III. SATELLITE-BASED QCS

The technical requirements of QCS, while not as stringent as most quantum communication tasks, does share many of the same features, e.g., the requirement of a sufficiently high entangled bit (ebit) rate between communicating parties. A significant amount of current research and development is focused on the use of satellites to go beyond the limitations of terrestrial fiber-based quantum communication networks. For example, the quantum repeaterless fiber optic-based secret key rate bound is surpassed beyond 215 km for a satellite at altitude of 530 km [31,32]. This means for distances beyond a few hundred kilometers between communicating parties, and in the absence of quantum repeaters, free-space communication via satellites will provide higher ebit rates. A key role in developing feasible long-distance quantum communication implementations has been played by the transition to hybrid space-terrestrial quantum communication network architectures combining satellites and ground stations equipped with optical telescopes with metropolitan scale fiber optic networks (see Fig. 2). This is because longer distance realizations of fully terrestrial quantum networks are hindered by the exponential losses associated with ground-based communication channels (primarily fiber optic cables) [7]. Unlike the classical information encoded in classical optical signals, the quantum information encoded via quantum communication protocols cannot be amplified due to fundamental limits on copying quantum information. This places fundamental limits on directly transferring quantum information through lossy channels. A large number of high-fidelity quantum repeaters and/or quantum memories could improve the situation to some extent, but their current performance levels are below those needed for mature applications [32] and, furthermore, it would very likely be impractical to place such devices in difficult terrain, e.g., mountains or oceans.

Recent free-space QKD experiments over long distances [33–35] and seminal experiments through the Micius satellite have indeed shown the effectiveness of a satellite-based quantum communication channel for large-scale quantum networks [31,36,37]. We quote a most striking observation from this seminal work to point out the inevitability of shifting to satellite-based platforms: “As a comparison, using the

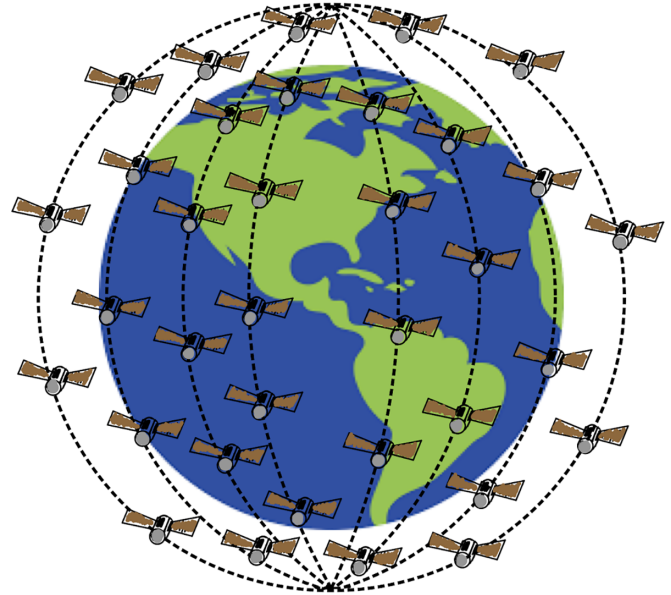


FIG. 2. A constellation of satellites used for global time distribution. Each satellite is equipped with an entangled photon-pair source along with photodetectors and transceivers (figure adapted from Ref. [7]). The satellites transmit and receive quantum signals to and from ground stations through a bidirectional quantum communication channel (downlink and uplink channels), which is used to synchronize onboard satellite clocks with terrestrial clocks using the QCS protocol mentioned in Sec. II.

same four photon sources and sending the teleported photon through a 1200 km telecommunication fibre with loss of 0.2 dB km^{-1} , it would take 380 billion years (20 times the lifetime of the Universe) to witness one event, assuming the detectors have zero dark counts” [36] (It is assumed that quantum repeaters are not used. Progress has been made toward implementing quantum repeaters but the technology is far from mature [32]). Other groups are also currently working to use small satellites to perform basic quantum communication tasks such as quantum key distribution (QKD) [32,38].

Consider now that Alice and Bob are separated in a way that makes it inefficient to exchange photons directly between the two parties. A quantum network between different cities is an example of such a scenario. The distances are large enough ($\approx 1000 \text{ km}$) to make direct communication through standard optical fiber channels (even with repeaters) less efficient and resource consuming than communication through a network of intermediary satellites in low Earth orbits. The satellites are to be used as intermediaries in the sense that ground station A can be synced to a satellite and then the same satellite could be synced to ground station B. This can either happen simultaneously, as shown in Fig. 3, or if the ground stations are too far apart, the two clock offsets can be sequentially estimated and compared after the satellite passes within range of both. In the latter case, the maximum time allowed between sync at stations A and B is determined by the stability of the satellite clock and is quantified by the hold over time τ . If all three clocks involved are relatively stable within the time this protocol is executed, then the clocks at A and B can be successfully synchronized in either case. This time includes the acquisition times (T_a) needed for individual sync events

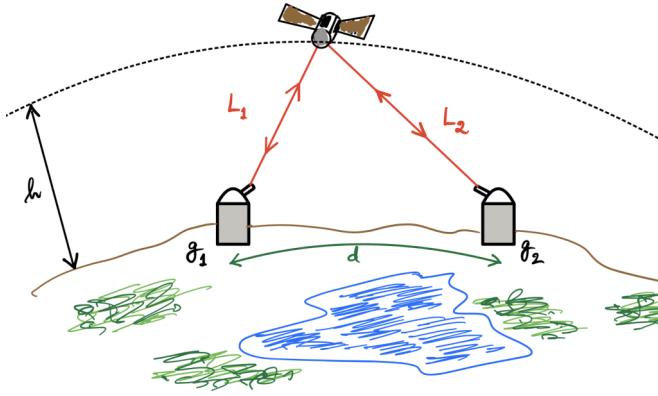


FIG. 3. Dual-link depiction for simultaneous clock synchronization between two ground stations (g_1 and g_2) with geodesic distance d between them (adapted from Ref. [7]). A LEO satellite at altitude h with asymmetric link distances L_1 and L_2 to the two ground stations.

at A and B plus the hold over time τ . Thus, the elementary task of this protocol is to synchronize a ground station and a satellite. In other words, we do not consider intersatellite communication, and therefore the sync between two ground stations must be established through a common satellite. This situation is of interest as a low-resource way of synchronizing users that span up to a continent-sized geographical area—e.g., a handful of select cities across the contiguous U.S.

In the discussion above, we have assumed a static situation with no motion between Alice and Bob. In the case of inertial relative motion the effect will be to spread out the correlation function by an amount proportional to the time over which the estimate is made, i.e., over the acquisition time. This acts essentially as an additional effective clock drift between Alice's and Bob's clocks. The length of the required acquisition time, the time-stamp resolution, and the relative velocity, will determine the effect that the motion has on the cross-correlation peak. If the relative velocity is known to within a maximum error, then the time-stamp data can be corrected to compensate for this “stretching” effect with some residual uncertainty. For example, if the relative velocity is known to a maximum error of 1 cm/s, for an acquisition time of 250 ms, the residual uncertainty in the correlation peaks will be less than 10 picoseconds (assuming that for short enough acquisition times the relative velocity remains constant). On the other hand if the relative velocity is not known to high precision, a parameter search can be performed over the time-stamp data to estimate both the velocity and the constant clock offset using methods already indicated in Ref. [1].

IV. SIMULATION RESULTS

The analysis of a QCS network as described in Secs. I and III is a complex task given that there are a number of variables involved. At the level of the fundamental QCS link between a satellite and ground station, one must first analyze the role of hardware parameters such as receiving and transmitting telescope radii, detector efficiencies, clock stability and source rates, etc. At the same time, one must also model a dynamic quantum communication link, since the satellite-

ground station distance is constantly changing (also a satellite is not always visible from a given ground station), effectively changing the transmissivity of the channel. Further, at the level of the network, the number of design parameters such as number of satellites, orbit selection (altitude, inclination etc.) is also large. This complexity makes this problem suitable to be computer simulated and we use this route to model the dynamical quantum communication link and to analyze quantitatively the performance of various network configurations or designs. As we discuss in detail in the next section, our code has the ability to simulate different scenarios in terms of resource constraints. The code is written in Python and uses parallelization in order to simulate large network sizes with tens of satellites and several cities across the globe.

Section IV A describes our simulations to characterize the performance of the QCS protocol for the purpose of synchronizing ground stations via small Low Earth Orbit (LEO) (also MEO) satellites. We will simulate the real-time motion of satellites relative to ground stations and obtain the periods of time along the day over which synchronization is possible. To quantify the capabilities of the network, rather than computing the cross-correlation functions described in Sec. II A, we will use quantum data communication rates [measured as entangled bits (ebits) shared per second] between satellites and ground stations as a proxy for sync precision. We will require a minimum ebit threshold for the sync to be able to occur at all. The use of ebit rates is highly convenient, since it provides an efficient tool to compute coverage area for time distribution from each satellite. This allows us to perform the simulations for a large number of network nodes (ground stations) and over long timescales, since the cross-correlation functions need not be simulated photon by photon. Nonetheless, we will justify *a posteriori* the use of ebit rates as proxy for sync precision through static simulations in Sec. IV C.

A. Dynamic simulation

This scenario takes into account the motion of satellites and ground stations around the globe to evaluate the periods of time along the day that ground stations are in view of satellites. This is done at the level of quantum data communication rates (ebits shared per second) without looking at the actual correlation functions. As summarized above, ebit rates are used as a proxy for the level of achievable precision, using the intuition that larger ebit rates correspond to higher correlation function peaks and hence higher precision. This intuition is backed up by static simulations in Sec. II A, where the actual correlation functions are simulated. As we show ahead, our simulations provide useful estimates for the capabilities of the network, in terms of the quantity of resources (number of satellites, number of orbits, etc.) needed to perform specific sync tasks. The results from Table III in Sec. IV C indicate that for the range of link losses encountered for a LEO orbit (500 km altitude) the protocol is always successful if the ebit rate is greater than approximately 200 ebits/s. From these observations, it follows that, if the sync is considered successful only if the clock offset can be evaluated better than (or equal to) 1 ns precision, then setting the cutoff for the quantum communication rate between the ground stations and satellites at 200 ebits/s ensures success of the protocol. The

small acquisition time requirement (250 ms) also justifies the use of ebit *rates* as a proxy for sync precision.

1. Details of the simulation technique

Our first goal is to apply the protocol described above to synchronize a satellite (Alice) and a single ground station (Bob) via a bidirectional quantum communication channel, i.e., a downlink and an uplink, and then use it to synchronize two ground stations that come in view of the same satellite.

We need to address two sets of questions: (i) characterization of the quantum communication channel, which will ultimately limit quantum data rates, and (ii) the dynamics of orbiting satellites. First, we look at the quantum communication channel between a ground station and the satellite. For concreteness, let us focus on a downlink channel; similar results hold for the uplink. We consider only a lossy channel assuming clear skies and ignoring any background noise from spurious sources—this can be incorporated later by introducing SNR thresholds or by choosing a higher cutoff rate.² Photons are either transmitted through the channel or lost in transmission. We characterize various loss mechanisms by their transmittance values η , which is the fraction of the received optical power to the transmitted power. The dominant sources of loss are (i) beam spreading (free-space diffraction loss, pointing error, etc.), $\eta_{\text{fs}}^{\text{down}}(L, h)$, (ii) atmospheric absorption or scattering, $\eta_{\text{atm}}^{\text{down}}(L, h)$, and (iii) nonideal photodetectors on the satellite and on the ground, with efficiencies given by κ_{sat} and κ_{grd} , respectively. The superscripts refer to the downlink. The transmittances are functions of the link distance L (physical distance) between satellite and receiver and h which is the satellite altitude. Simple, analytic formulas are used to estimate $\eta_{\text{fs}}^{\text{down}}$ and $\eta_{\text{atm}}^{\text{down}}$, following Ref. [7]. Then, given an onboard source which generates entangled photons at an average rate of \mathcal{R} ebits per second, we can estimate the quantum data communication rate (ebit rate) between a satellite and a ground station for the downlink by

$$\mathcal{R}^{\text{down}} = \mathcal{R} \eta_{\text{fs}}^{\text{down}} \eta_{\text{atm}}^{\text{down}} \kappa_{\text{sat}} \kappa_{\text{grd}}.$$

The precision to which Alice and Bob can synchronize their clocks depends on the amount of successfully detected, correlated photons transmitted through the bi-directional communication channel over some acquisition period. Hence, the quantum data rate pair $\mathcal{Q} := (\mathcal{R}^{\text{down}}, \mathcal{R}^{\text{up}})$ serves as a useful performance metric for the clock synchronization protocol. We generalize this to a network of satellites and ground stations by indexing the quantum data rate pair as \mathcal{Q}_{ij} , where the first index corresponds to the i th satellite and the second index corresponds to the j th ground station.

Next, we incorporate dynamics into the communication channel. Since the satellites are in motion with respect to the ground stations, the quantum data rates will generically change as a function of time, since the transmittance values are a function of the physical distance L (and visibility)

²While estimating the cutoff rate using static simulations in Sec. IV C, a dark count rate of 1000 Hz was assumed, hence the cutoff rate $\mathcal{R}_c = 200$ ebits/s includes the effect of noise due to dark counts. Similarly, the effect of stray light can be included by raising the cutoff further.

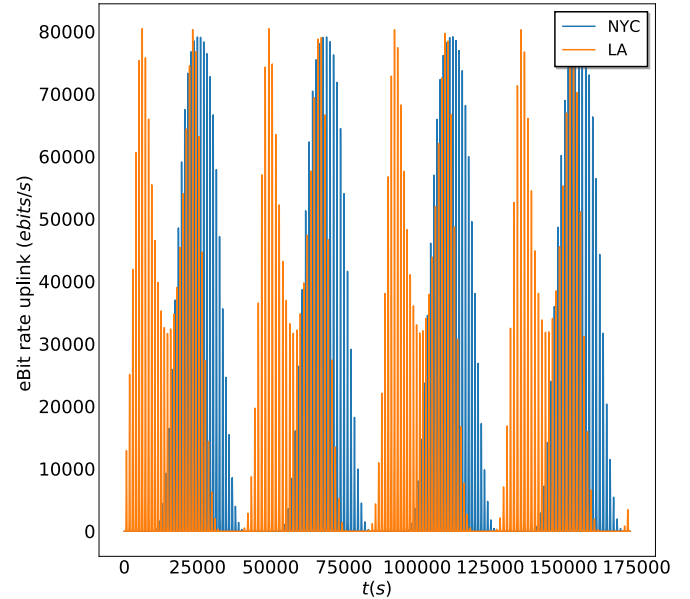


FIG. 4. Connection traces (uplink ebit rates) for two cities in the U.S.: New York City (blue—light grey line) and Los Angeles (red—dark grey line). The satellite network is comprised of ten satellites—two tilted polar orbits (50° and -50° to the Earth’s axis of rotation) of five satellites each in a 500 km LEO. Connection is considered established when the ebit rate exchanged between the satellite and ground station is greater than the cut off rate of 200 ebits/s. Each sharp vertical line corresponds to a single satellite pass (which would be a broader curve if we zoomed in to a smaller timescale), and consecutive vertical lines correspond to passes of consecutive satellites within an orbit. The bunching of vertical lines is due to the fact that there are many satellites in each orbit. The recurrence of this bunch occurs after a six-hour period (approximately 20 000 seconds after the first bunch in the trace), when an orbit comes in view of the cities. The separation between the peaks for the two cities indicates the fact that satellites pass over these cities at different times.

between the satellite and ground station. For simplicity, we assume circular orbits for all satellites. We adapt and extend software previously created by authors in Ref. [7] to simulate satellite and ground-station motion and compute physical distances between them as functions of time. These distances are then used to evaluate transmittances and the quantum data rates \mathcal{Q}_{ij} . For more details regarding the physical aspects of these simulation techniques, see Appendix A. In our simulations, the parameters describing the hardware design have been reasonably chosen based on recent demonstrations [31,38] and are representative of the current state of the art. The operating wavelength of the sources was chosen to be 810 nm, while the source strength was set to 10 million pairs per second. The detectors onboard the spacecraft are assumed to be noncryogenic, passively quenched, Geiger-mode avalanche photodiodes (GM-APDs) that are 45% efficient at a wavelength of 800 nm. For this design study, detector efficiencies were set to 50% as a representative value for a broad class of APDs. Lastly, the apertures for the satellite and ground-station telescopes were chosen to be of 10 cm (fill factor of 80%) and 60 cm, respectively, which represent typical optical communications sizes that are used for classical LEO laser

communications [39–41]. Apart from these fixed hardware parameters, we also have several other variable parameters such as orbit altitude, number of satellites, distribution of satellites among orbits, orbit inclination, stability of satellite clocks (quantified by the hold over time τ), and cutoff rates \mathcal{R}_c .

We study the effect that a change in these parameters has on the performance of the network, which we assess through a few simple figures of merit defined in the following sections. The fundamental output of our simulations is the *connection trace* between satellites and individual ground stations, which is the quantum data communication rate for uplinks (which is always weaker than the downlink, primarily because of the smaller receiving telescope onboard the satellite) as a function of time. For example, Fig. 4 shows the connection trace for uplinks from New York and Los Angeles to a constellation of ten satellites distributed equally into two tilted polar orbits.

The connection traces provide information about the number of ebit pairs available at any given time that could be utilized to synchronize a ground station with a satellite.

$$Q_{1j}(t) = \begin{cases} Q_{1j}(t), & \text{if } Q_{1j}(t) > \mathcal{R}_c \text{ and } \max_{\{t-\tau < t' < t+\tau\}} \{Q_{2j}(t')\} > \mathcal{R}_c \\ 0, & \text{otherwise.} \end{cases}$$

The sync traces for New York City and Los Angeles (for the same satellite configuration used in Fig. 4) are shown in Fig. 5 for a hold over time of 600 seconds (standard rubidium clocks can hold time at 1 ns precision for around 600 s, even smaller CSACs can do so for around 60–100 s. For reference, an ordinary quartz crystal wrist watch can hold time at around 1 ms precision for 100 s [42]). Simply put, sync traces are chopped up versions of the connection traces, indicating regions of simultaneous connection (or nonsimultaneous but within time τ of each other). Larger τ implies more common connections (also see Fig. 9).

Analyzing these connection traces and sync traces, we can address questions regarding the performance of the time distribution protocol under varying practical constraints. Some of which are: How do the quantum data communication rates change with satellite altitude and other input parameters? If there are resource constraints on the quantity of satellites in orbit and constraints on the quality of their onboard components, to what precision can two ground stations synchronize, and how often can this synchronization be accomplished? Given various satellite configurations (e.g., using polar orbits or different constellation designs), how often do users in specified geographical areas have access to the time distribution service per day? Such questions are complicated to answer generically due to the large parameter space that we need to explore to address them and due also to the nontrivial interdependence of these inquiries. In the subsequent sections, we provide specific tools and techniques which we can leverage to address these questions and also provide analyses for specific case studies.

We begin our analysis by illustrating the effect of satellite altitude h on the ability to make ground station connections and exchange entangled bits. Network scale is determined by

Nonetheless, all these ebits are not useful for the synchronization between two ground stations. To estimate the sync quality between two ground stations, we must only consider ebits which are shared between two ground stations and a common satellite. To that end, from the overlap between connection traces of two cities we can compute *sync traces*. This overlap can be either instantaneous or over a time window τ , where τ is equal to the hold over time of the clock onboard the satellite. More concretely, the sync trace for a city is different from zero at a given time only if the other city also receives an ebit rate above the threshold from a common satellite. This can happen if a common satellite has been in view of both cities within a time interval τ . If Q_{1j} and Q_{2j} are the uplink ebit rates from ground stations 1 and 2 to some common satellite (index j), then the sync trace $Q_1(t)$ for city 1 is given by (also similarly defined for city 2):

$$Q_1(t) = \max_j Q_{1j}(t),$$

where

the largest distance between ground stations that can be successfully synced at subnanosecond precision. As mentioned earlier, this is achieved whenever communication between the satellite and both ground stations is simultaneously achieved at an ebit rate greater than \mathcal{R}_c . Since uplinks are weaker than downlinks, they determine the success of the network. Figure 6 summarizes the average entangled bit rate over one day as a function of ground-station distance separation for differing satellite altitudes. Two ground stations are placed equatorially some distance d apart with one equatorial satellite placed overhead (as depicted in Fig. 3). For a given satellite altitude h , the ebit rate averaged over the course of a day is recorded (the product of two uplink ebit rates from each ground station to the satellite is used, which is the same as assuming $\tau = 0$). This procedure iterates with varying ground-station separation distances and satellite altitudes to create this figure. We see for low altitudes more entangled bits are exchanged when the ground stations are relatively close together, as one would expect. But as ground-station separation passes 3000 km, the lowest altitude satellite is no longer able to establish connection and, consequently, no ebits are exchanged (if the average ebit rate is zero, the instantaneous rate must also be zero all through the day). As the orbit is moved to higher altitudes, this does allow for the satellite to connect simultaneously to more distant ground stations, but at the cost of losing some fraction of ebits due to increased transmission losses. It is clear from Fig. 6 that there is a trade-off in choosing satellite altitudes that depends on the objective of the timing network. While a lower satellite can effectively deliver a higher bit rate due to smaller transmission losses, the amount of time ground stations can remain in view of the satellite diminishes, particularly as the ground stations become more distant.

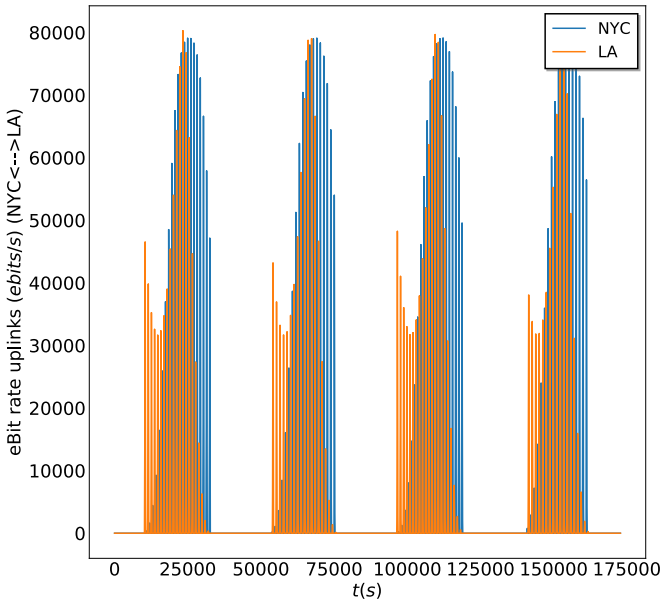


FIG. 5. Sync traces for a pair of cities in the U.S.: New York City–Los Angeles. The satellite network is comprised of ten satellites—two tilted polar orbits (50° and -50° to the Earth’s axis of rotation) of five satellites in a 500 km LEO. The sync trace of a city is nonzero only when it is in view of a satellite (with ebit rate above the threshold), and the other city from the pair has also been (or will have also been) in view of the same satellite within an interval equal to the hold over time of the clock onboard the satellite. For this figure, $\tau = 600$ s. Sync traces are chopped up versions of the connection traces, indicating regions of simultaneous connection (within a τ window). Compare with Fig. 4.

To further expound the effects of satellite constellation altitudes as well as ground-station separation distances, we look at Fig. 7 to compare the change in the amount of time the satellite is simultaneously connected to both ground stations when varying these parameters. As in Fig. 6, equatorial ground stations are incrementally separated and attempt synchronization through an equatorial satellite orbiting at a particular altitude. The ratio of time that the satellite is connected to the two ground stations divided by the total time within one orbital pass (roughly 90 minutes) is plotted. This is done for several satellite altitudes over a separation distance between ground stations in the interval 500 and 5000 km. Of note here is that the connection time ratio scales linearly as a function of ground-station distance up until connection can no longer be established. Also, as satellite altitude is increased, this time ratio increases as the ground stations continue to stay in view of the satellite for longer. This highlights that if establishing connections for longer times with at least some minimum number of exchanged entangled bits is favored over having an increased number of exchanged ebits in far apart smaller time windows, satellite constellation altitude is one parameter to consider.

It is clear from Fig. 6 that for a given satellite altitude and cutoff rate, there exists a critical distance beyond which two ground stations cannot connect to the same satellite. This motivates us to introduce an intuitive visual tool to understand the previous plots in a simple manner, alleviating some of the complexity originating from the large number of parameters

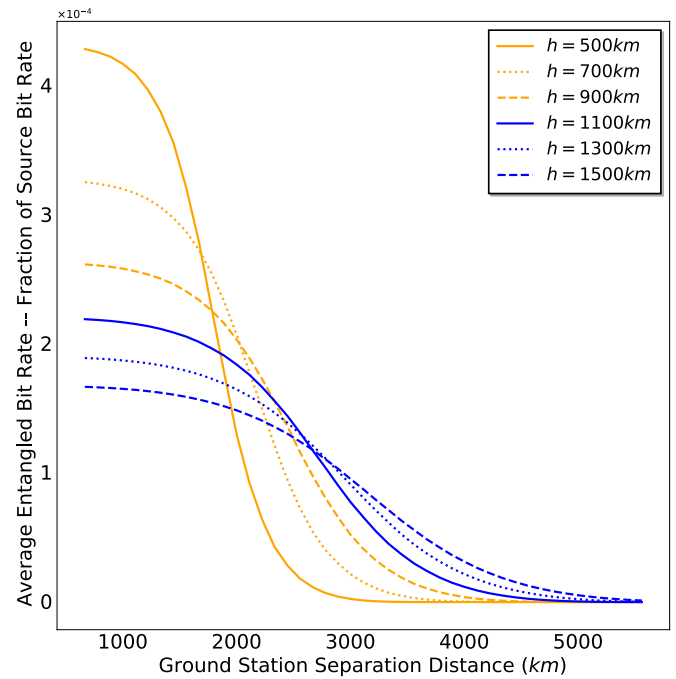


FIG. 6. Average ebit rate (of the product of two uplink rates) calculated over one day as a function of the arc distance separation between two ground stations for different satellite altitudes, for a value of $\tau = 0$ (poor onboard clock). The two ground stations lie along the equator and the satellite is also in an equatorial orbit. A sharper drop-off is seen for low satellite altitudes while for larger altitudes the drop is less pronounced. In this double-link configuration, we see good performance for ground-station separation distances at or below 3000 km but a sharp drop in performance above this range.

involved. Consider a single satellite. At a given time, it will be able to synchronize with all ground stations for which it has a ebit exchange rate larger than the threshold $\mathcal{R}_c = 200$. But since the exchange rate decreases with the satellite-to-ground station distance, this threshold can be translated to a region on the surface of the Earth below the satellite, which we call the shadow. As one moves toward the center of the shadow, concentric regions indicate regions of better sync precision. Hence, the higher the cutoff rate \mathcal{R}_c , the smaller the shadow. With this picture in mind, it is easy to understand that two ground stations would be able to sync at a given level of precision by means of an intermediary satellite whenever they both simultaneously fall under the satellite’s shadow. Furthermore, if the clock onboard the satellite is able to hold time at the required precision for an interval τ , the shadow effectively elongates, covering a larger area on the Earth’s surface directly proportional to τ . See Fig. 8. Since LEO satellites are fast moving (≈ 8000 m/s), even small values of τ translate to large ground-coverage areas. For the effect of satellite clock stability on the sync traces, see Fig. 9.

Next, we briefly discuss the effects of increasing the number of satellites in a particular orbit, the number of orbits utilized, and the orbit type (or inclination from the Earth’s axis of rotation) on constellation design. In Fig. 10, satellite-to-ground sync traces are provided between two ground stations based in Atlanta (ATL) and NYC for a varying number of satellites in a single LEO, over the course of a two-day simula-

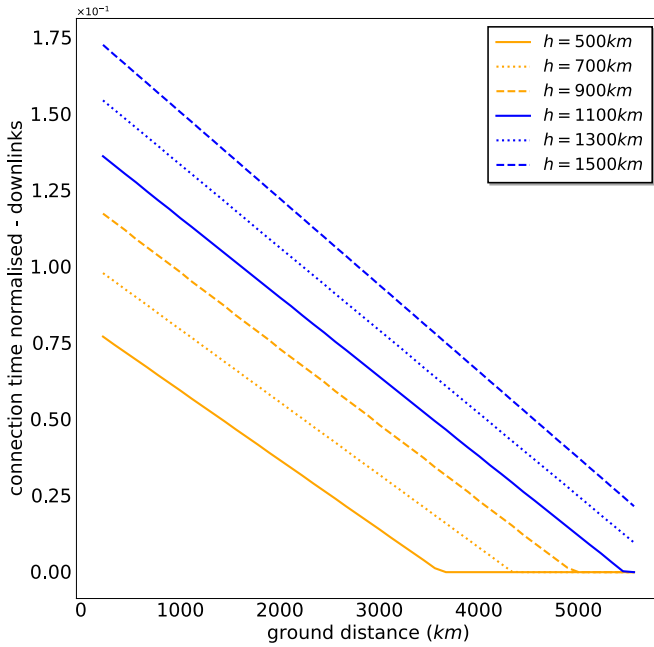


FIG. 7. Ratio of connected time to the total time for a single orbital pass (~ 90 min) as a function of ground station arc distance separation for different satellite altitudes. A linear relationship is seen for all altitudes. The average connection time increases with increasing altitude, but average ebit rates fall (Fig. 6).

tion. As the number of satellites is increased, the opportunity for connections to occur also increases up to a threshold. Beyond this point, adding additional satellites for a particular ground station pair does not increase the connection time, although it does allow for higher ebit rates. The particular satellite chosen at each instant to sync the ground stations is based on which provides the least transmission loss at that particular time. Further, in Fig. 11 we show the effect of orbit inclination on the sync trace between NYC and LA. By orienting the satellite shadow along the line joining the two cities network, one can improve outcomes such as quantum data rates, connection time averages, etc.

The previous discussion illustrates the complexity of the problem of optimization of a network of satellites arising from the vast space of parameters. The study of the design space are, in part, predicated on which ground stations are important to synchronize, whether some quality of service is to be expected at individual locations, and what type of constraints in terms of costs or resource availability are actually considered in the construction and launch of such a constellation. This leads us, in the next subsection, into considering a concrete network scenario and exploration of time distribution within the imposed constraints.

B. A QCS network for continental U.S.

As a concrete scenario, we consider the requirement to synchronize cities lying within the continental United States (see Fig. 12) at a subnanosecond precision. The constraints are the availability of moderately stable satellite clocks onboard (τ of a few minutes), a small number of LEO satellites, and the

absence of quantum communication links between satellites (satellites can only communicate to ground stations)

We assess the performance of our network by the following two criteria:

(i) How well can we synchronize? We quantify this by the *average uplink and downlink loss* when a connection is established between a satellite and a ground station. The intuition is straightforward: lower loss leads to a higher number of ebits exchanged, which leads to better statistics for the timing offset calculations; see Sec. II A. This all, in turn, leads to higher precision of the QCS protocol.

(ii) How often can we synchronize? Or, similarly, how often do a pair of ground stations get a common satellite in view? The longer the gap between two synchronization events is, the more stable a ground-station clock must be to maintain synchronicity. To address this notion of revisits quantitatively, we introduce the *connection time fraction*, calculated as the fraction of time a satellite is connected to the ground station divided by the total simulated time, and the *longest connection time gap*, calculated as the longest time interval a ground station has to stay without a connection to a satellite. The higher the connection time fraction, the higher the total number of ebits shared between the satellite and the ground station. We point out that, when synchronization occurs more frequently (e.g., higher satellite traffic over some terrestrial region), ground stations can leverage lower quality clocks if desired (compared to other ground clocks which sync after long gaps of time and hence must have long stability (hold over) periods). Hence, appropriately addressing questions of revisits can also help to relax certain resource requirements.

For this concrete requirement, we assess the feasibility of synchronizing ground stations located at the four corners of the contiguous United States (NYC: New York City; LA: Los Angeles; SEA: Seattle; ATL: Atlanta). To begin, let us consider a single satellite in a tilted orbit (-50° angle compared with the Earth's axis of rotation) with a modestly stable onboard clock; $\tau = 500$ s. This constellation configuration, as sparse as it is, does allow for successful QCS among the four cities, as long as the local ground-station clocks are sufficiently stable. The average uplink signal loss for ground station pairs range between 27 and 32 decibels. The downlink losses range between 23 and 30 decibels, slightly lower than the uplink losses due to smaller receiving telescope aperture on the satellite³ (also see Refs. [31,43] for experimental and simulation results reporting similar values of the loss). For a source emitting 10^7 entangled pairs per second and a satellite at 500 km altitude, this translates to between 10 000 and 15 000 ebits exchanged per second on average; roughly 10^5 ebits total per satellite pass. Since we are using a single satellite, the connection time percentages are low and range between 1.3% and 2.8% of a day; i.e., between 20 and 40 minutes in total. The longest disconnected intervals between revisits by the satellite range from 15 to 20 h. So, ground stations whose clocks have a relative frequency drift no bigger

³Also, dispersion effects in lower atmosphere lead to beam broadening; this would affect the uplink losses more. We do not consider the effects of turbulence in our simulations.

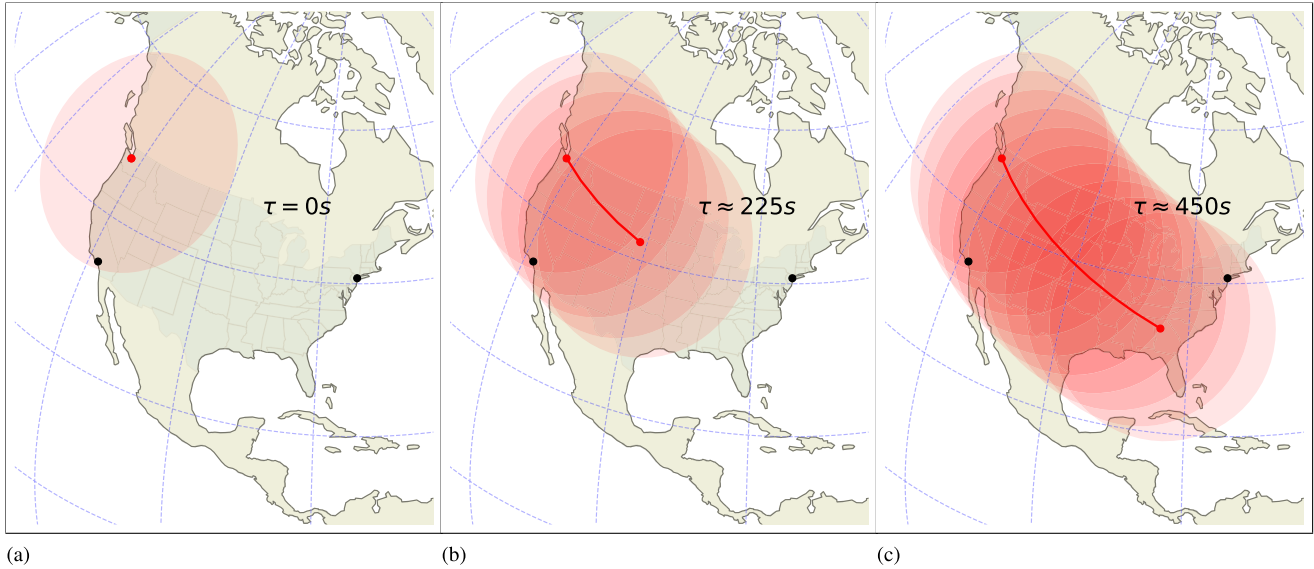


FIG. 8. Illustration of the shadow of a satellite, and the effect of varying hold over time (τ). For the limiting case of no hold over time (a), only what the satellite (red dot) has under the instantaneous shadow may be connected and synchronized. As the time window is increased to $\tau \approx 225$ s, the satellite track length increases (red line) and includes more distant locations that can then connect and synchronize (b). In this representation, as the hold over time is increased to $\tau \approx 450$ s (c), ground stations (black dots) LA and NYC can be synchronized with one another. (Figure is not to scale.)

than 1×10^{-14} connected via this type of constellation—one satellite—can provide quantum time transfer capabilities down to 1 ns precision. Therefore, using our simulations we find that an orbit tilt of around 50° about the equatorial plane can provide coverage across the entire contiguous U.S. (also see Fig. 11). For larger values of τ , a smaller tilt is required and vice versa. Thus, we show that we are able to extract information about the orbit resources (orbit space and orientation) needed to service specific geographical regions. In effect, this allows us to establish generic network sizes in terms of geographical area covered by the network. This could also be intuitively understood using the shadow picture developed earlier in the section. In this specific case, choosing $\mathcal{R}_c = 200$ ebits/s and $h = 500$ km translates to approximately 35° angular diameter for the shadow spot, and the choices of $\tau = 100$ s and $\tau = 600$ s give angular lengths of the shadow equal to around 38° and 75° , respectively (which translate approximately to distances of 4000 km and 8000 km, respectively). Now, consider the contiguous U.S.: The longitudinal extent of the cities considered here is around 50° and the latitudinal extent is only around 15° . The shadows of polar satellites with no tilts, in this case, will have longitudinal and latitudinal extents of around 35° and 75° , respectively. Hence, an orbit tilt of around 50° [$\arccos(50/75)$] about the equatorial plane orients the shadow so as to cover the entire contiguous U.S.

Next, Table I provides the results for a satellite constellation of two tilted orbits (50° and -50° to the Earth's axis of rotation) of five satellites each with the same ground stations as above. A larger τ allows not only for lower signal losses but also higher connected time percentages and shorter revisit times. This effect is more pronounced for ground stations with larger separation distances. The takeaway is that the stability of a satellite's onboard clock can markedly enhance the geographical extent to which ground stations can

be synchronized. On the other hand, a larger ebit threshold reduces the connected time percentages and elongates revisit times. All these results can be intuitively understood by using the picture of the shadows of each satellite, and the way the shadow changes with both the ebit rate threshold \mathcal{R}_c and the hold over time τ , already explained in the previous section.

Further, in Table II we summarize the figures of merit for a similar MEO (medium Earth orbit) constellation at 5000-km altitude. Clearly, at the expense of having larger losses, longer connectivity can be obtained. (This, however, should not be thought of as a trade-off between sync precision and the size of the coverage area, since whenever the ebit rate is above the threshold value the required precision can be achieved.) Due to larger instantaneous shadows cast by MEO satellites, to cover a similar geographical area (contiguous U.S. in this case) the requirement on τ is much smaller (lower stability satellite clocks can be used).

C. Static simulation

The goal of these static simulations will be to quantitatively determine a practical lower bound (*ebit threshold*) \mathcal{R}_c for the ebit rate to yield a clock offset estimate at a certain precision. The simulation is static in the sense that the relative motion between the satellite and ground station is not included; rather, an appropriate fixed value for channel transmissivity is chosen [acquisition time required to perform the sync protocol is small ($T_a \approx 250$ ms), the link distance and hence the losses do not change at this time scale]. Monte Carlo simulations are performed to generate photon time stamps and thereby the correlation functions defined in Sec. II A. However, relative clock drift can be included in the simulation.

The static simulation of the performance of the QCS protocol uses a Monte Carlo simulation of the photon pair

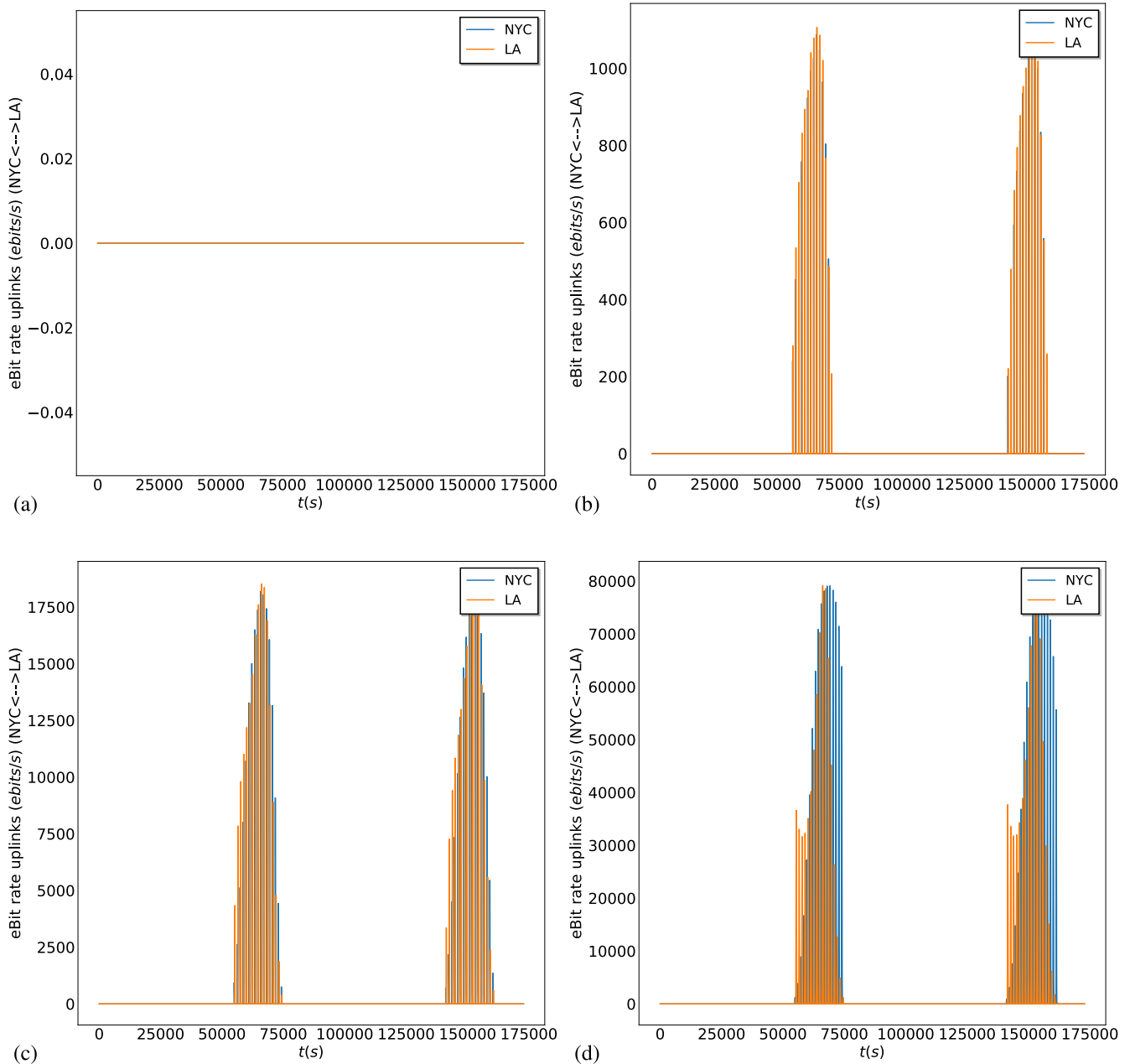


FIG. 9. Satellite-to-ground sync traces for Los Angeles (red line) and New York City (blue line) as the hold over time τ is increased from (a) hold-over time $\tau = 0$ s, to (b) $\tau = 100$ s, (c) $\tau = 200$ s, and finally, in (d) $\tau = 600$ s. While τ remains low, it is not possible for these ground stations to synchronize. As clock performance onboard the satellite is improved and τ increases, the potential for synchronization (eBit rate) as well as the overall time connected increases. (One orbit of -50° tilt with five satellites at 500 km altitude is used for this depiction.)

production, the link loss, photon detection, and detection time stamping. The simulation parameters include the time-correlated photon pair source rate (Poisson-distributed pair production with a specific rate), the (fixed) losses in the optical links (dB), detector efficiencies (fixed, no dead time is modeled), detector dark count rates (Hz), timing jitter (ps, FWHM), time-stamp resolution (ps), the clock drift rate for each clock (fractional frequency accuracy), and the total acquisition time during which the photons are detected (seconds). For each set of these parameters, a different true clock offset is uniformly randomly chosen in the interval between 0 and 1 ms and 100 different time-stamp data sets are generated

for each value. Thus, we simulate 100 instances each for a range of QCS scenarios each with a fixed clock offset. Once the time stamps are generated and detected in each instance, fast Fourier transforms (FFTs) of the resulting times series are performed to find the required cross correlation functions. Successful cases are those whose simulated clock offset estimate is within 1 ns of the true value.

Although the simulation is static in that there is no relative motion between the two clocks, a constant velocity between them will have the effect of inducing an apparent relative clock drift between the clocks. The relative velocity between ground stations and satellites can be considered constant if

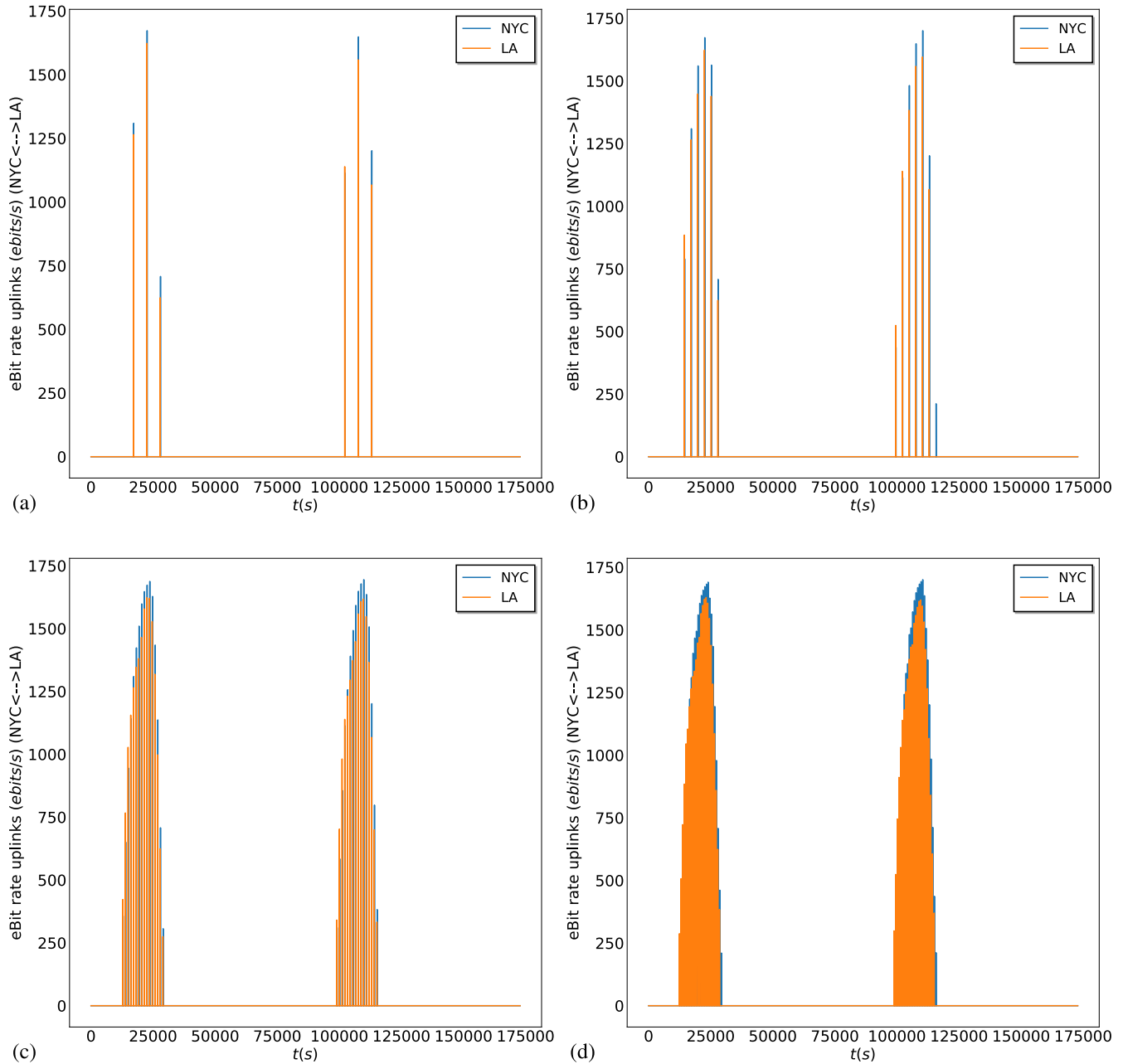


FIG. 10. Satellite-to-ground sync traces of New York City and Los Angeles (uplinks) as the number of satellites per orbit (1 orbit of -50° tilt at 500 km altitude and $\tau = 100$ s in this depiction) is varied from (a) $n = 1$ to (b) $n = 2$, (c) $n = 5$, and (d) $n = 8$. As the number of satellites increase in this particular configuration, the density of viable connections increases; see (a)–(c). Beyond a threshold number of satellites (five in this case), the amount of connection time does not benefit significantly (d).

the required acquisition time is small enough. Therefore, if this relative velocity is known to sufficient precision, the effect of motion can be corrected by applying a compensating transformation to the recorded time-stamp data. Alternatively, with a sufficient data rate, one can estimate both the clock offset and relative clock drift rate directly from the time-stamp data. In this way, only limited external information about the satellite's motion would need to be used. This would be preferred in the case that the time distribution network functions independently of GPS or other GNSS constellations. For more details about these techniques, we refer the reader to Ref. [1].

Note that the acquisition time (T_a) used for each independent clock offset estimate is limited by the effective (uncompensated motion induced plus intrinsic) relative clock drift rate. This is because if the effective drift rate times the acquisition time exceeds the time-stamp resolution, the height of the cross-correlation peaks rapidly begin to be reduced since the correlations become spread over many time bins in the FFT window used for the cross-correlation calculations. In the simulations, we have chosen an upper limit of $T_a = 250$ ms. For a time-stamp resolution of 50 ps, this means the clock synchronization algorithm will have no difficulty with a relative fractional frequency offset of 2×10^{-10} or less, as

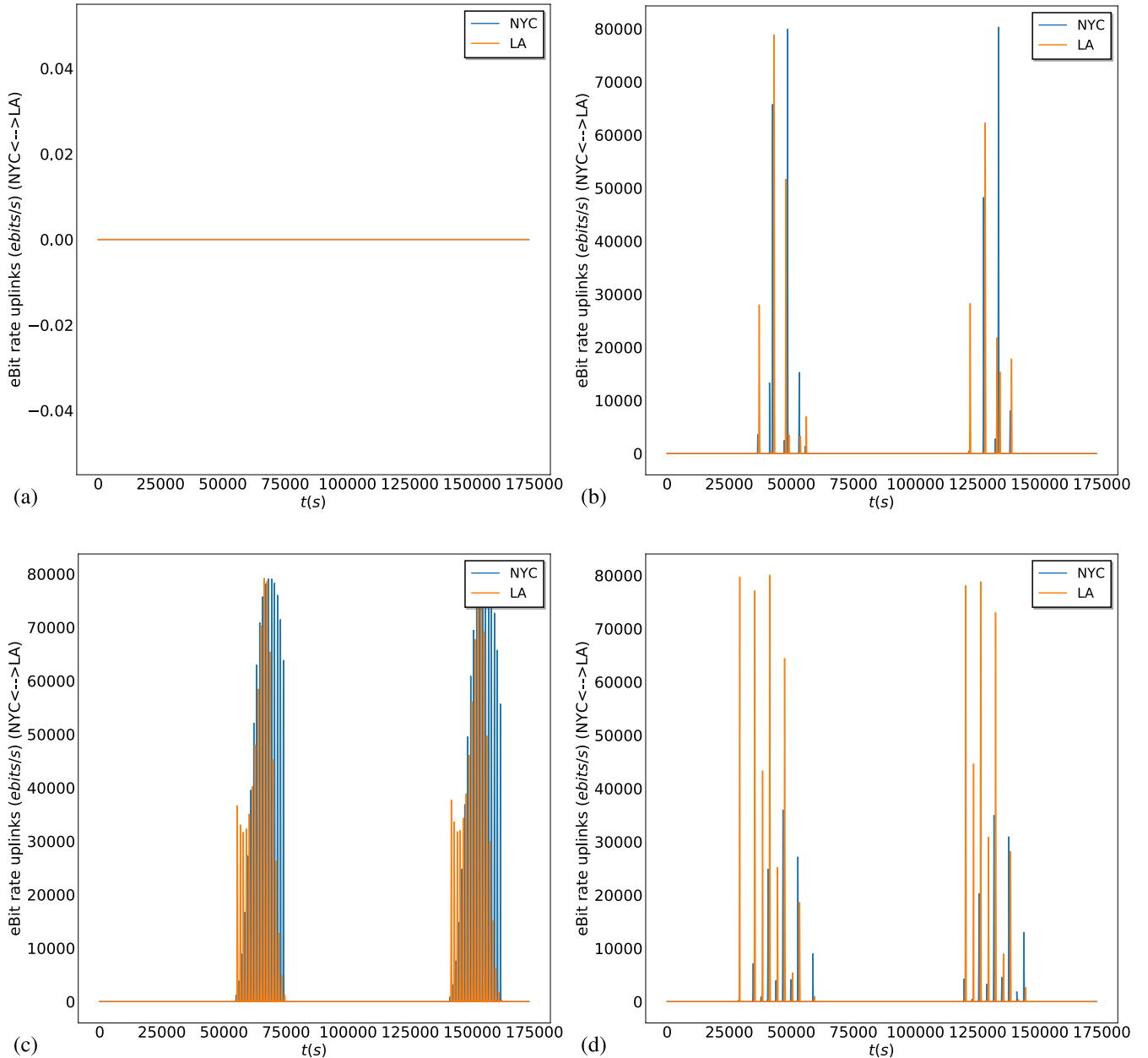


FIG. 11. Satellite-to-ground sync traces for New York City–Los Angeles as the orbit tilt is varied from (a) 0° to (b) 25° , (c) 50° , and (d) 75° (one orbit with five satellites at 500 km altitude, $\tau = 600$ s). By orienting the satellite orbit along the line joining the two cities, all network figures of merit, including quantum data rates, connection time averages, and longest connection gap, are improved. $\pm 50^\circ$ appears to be the optimal tilt for the orbits for this city pair. This is quantitatively justified below using the concept of the satellite shadow as well.

determined by the fractional frequency error of the clock. For reference, the frequency stability of a CSAC is about 3×10^{-10} measured over 1 s [8]. Therefore, assuming accurate enough compensation for the relative motion, the simulation results below should be consistent with those achievable when using clocks with short-term stability no better than provided by CSACs. Note that the frequency stability is measured in the time domain by the ADEV which is the uncertainty of the clock's frequency measured over a specified length of time. Since the acquisition time used in the simulations are on the order of 1 s or less, the ADEV at 1 s provides a useful upper bound on the frequency error as measured by the reference clock.

The results of the simulations with fixed acquisition time of 250 ms and varying link losses are given in Tables III–V. The parameters have been chosen to be representative of realistic components. The simulation sets each of the detector's efficiency to 50% with a dark count rate of 1000 Hz. We see in Table III that in the limiting case of no timing jitter (due to detectors and time stamper) and a time-stamper resolution of 50 ps, there is a sharp increase in failure rate of the clock offset estimation as the ebit rate drops below about 100 ebits/s. As can be seen in Table IV, with a realistic value of 100 ps for the timing jitter, the required ebit rate increases to about 200 ebits/s. When the number of exchanged ebits falls much below 50, the clock synchronization algorithm begins



FIG. 12. Selection of representative ground station cities in the contiguous USA. We choose four cities of >1 M people, separated by close to the maximum possible distance: Seattle, New York, Atlanta, and Los Angeles. The intercity distances (in km) are presented in the map.

to fail at least as often as it succeeds. Thus, for the chosen realistic parameters, an appropriate cutoff for the ebit rate is about 200 ebits/s with an acquisition time of 250–500 ms. In Table VI, we see the effect of changing the acquisition time for each offset estimate for a fixed value of the link loss. As the acquisition time is reduced from 250 ms, the number of successful offset estimates observed over the 100 simulations is reduced, while for longer acquisition times such as 500 ms, the effect of the frequency instability of the satellite clock increases the width of the cross correlation peak resulting in a SNR that is roughly identical to the 250 ms case and with reduced accuracy.

To increase the achievable clock synchronization accuracy, the individual estimates from each acquisition window can be averaged. This will reduce the random errors due to timing jitter and other random system noise as a function of the integration time. While for LEO satellites this integration time will be limited to a few hundred seconds, for many locations this should allow the synchronization accuracy to approach the time-stamp resolution. The stability of the clock on the satellite will also determine the length of optimal integration time since the uncertainty in the clock’s drift rate will place an upper bound on the optimum integration time.

V. SUMMARY OF RESULTS

The goal of this paper is to quantitatively evaluate the performance capabilities of a satellite-based scheme to perform clock synchronization between ground stations spread across the globe using quantum resources. We have developed a software infrastructure to simulate the evolution of a satellite network from which we can compute the real-time quantum data communication rates between ground stations and satellites. All aspects of the network regarding synchronization capabilities can be extracted from these real-time quantum data communication rates. To put these tools in

action, we have considered a representative example, consisting of assessing the feasibility of synchronizing ground stations located at the four corners of the contiguous United States (NYC: New York City; LA: Los Angeles; SEA: Seattle; ATL: Atlanta). We show through numerical simulations that a single satellite in a LEO orbit can provide 1 ns sync precision between ground clocks in such a network. The range of parameters chosen for this paper are either commensurate with off-the-shelf equipment or will be available for commercial use in the near-term. We then analyze the effect of different hardware and constellation design parameters on three key performance measures, the sync precision achieved, the scale of the network, and the time gaps between successive connections. The important takeaways in this regard are as follows:

(i) The sync precision achieved between clocks located in a given region on the Earth’s surface is determined by the rate at which ebits can be exchanged between the ground stations and a common satellite. Thus, setting an ebit rate threshold—minimum rate of ebit exchange between ground stations and satellites at which connection is considered established, translates to a requirement on minimum achievable precision, e.g., a threshold of 200 ebits/s translates to ensuring a sync precision of at least 1 ns between a ground station and a satellite (see Table III, 100% of simulations are successful with a mean error of less than 50 ps). Higher jitter, noise, and/or dark counts lead to a higher threshold requirement at the same level of precision (see Table IV). At a fixed level of jitter and noise, increasing the threshold translates to higher precision requirement. At the same time, since the ebit rate falls with increasing distance between the ground station and satellite, the network size falls if a higher threshold or higher precision requirement is considered. (See Table I.)

(ii) The stability of a satellite’s onboard clock can markedly enhance the geographical extent (network scale) to which ground stations can be synchronized, e.g., in the case of a single satellite in 500 km LEO orbit, if the satellite clock

TABLE I. QCS network figures of merit for ground station pairs in the contiguous US with a constellation of 10 LEO satellites (2 tilted polar orbits of 5 satellites each). Orbit altitudes are set to 500 km, ebit connection rate threshold \mathcal{R}_c and hold over time τ are varied. Average ebit losses for up and downlink are reported from each ground station in decibels (this includes detector inefficiencies ≈ 6 dB). An average loss of 30 decibels converts to a ebit loss fraction of 10^{-3} . Therefore, if the entangled source rate is 10^7 ebits/s then, on average, 10 000 ebits are detected between the satellite and ground station per second when a connection is established.

Ground station pair (GS1/GS2)	Average uplink ebit loss(dB/dB)	Average downlink ebit loss (dB/dB)	Percent of day connected	Longest connection gap (hours)
$h = 500$ km, $\mathcal{R}_c = 200$ ebits/s, $\tau = 100$ s				
NYC/LA	42/42	41/41	0.6%	17
NYC/SEA	44/44	43/43	0.1%	15
NYC/ATL	27/28	23/24	19%	6
LA/SEA	28/29	24/25	16%	6
LA/ATL	33/33	31/31	5%	6
SEA/ATL	39/37	37/36	1.5%	11
$\mathcal{R}_c = 200$ ebits/s, $\tau = 200$ s				
NYC/LA	33/33	23/24	3%	10
NYC/SEA	36/38	24/30	2%	16
NYC/ATL	27/28	24/24	21%	6
LA/SEA	28/29	24/26	19%	6
LA/ATL	28/28	24/25	8%	6
SEA/ATL	33/30	29/25	4%	8
$\mathcal{R}_c = 200$ ebits/s, $\tau = 500$ s				
NYC/LA	27/28	23/24	11%	16
NYC/SEA	28/31	23/29	8%	16
NYC/ATL	27/28	23/24	21%	6
LA/SEA	28/29	24/25	19%	6
LA/ATL	28/28	24/24	15%	6
SEA/ATL	31/28	27/24	12%	10
$\mathcal{R}_c = 500$ ebits/s, $\tau = 100$ s				
NYC/LA	42/42	41/41	0.1%	21
NYC/SEA	∞/∞	∞/∞	0%	∞
NYC/ATL	26/27	22/23	17%	6
LA/SEA	28/28	24/25	15%	6
LA/ATL	33/33	31/31	3%	7
SEA/ATL	38/37	37/36	0.8%	18
$\mathcal{R}_c = 500$ ebits/s, $\tau = 200$ s				
NYC/LA	33/33	31/31	2%	17
NYC/SEA	36/37	35/36	1%	16
NYC/ATL	27/28	23/24	19%	6
LA/SEA	28/28	24/25	17%	6
LA/ATL	28/28	25/25	7%	7
SEA/ATL	33/30	31/28	3%	17
$\mathcal{R}_c = 500$ ebits/s, $\tau = 500$ s				
NYC/LA	27/27	23/24	9%	17
NYC/SEA	27/31	23/29	7%	16
NYC/ATL	27/28	23/24	19%	6
LA/SEA	28/28	24/25	17%	6
LA/ATL	27/28	24/24	13%	7
SEA/ATL	30/28	27/24	10%	10

has no ability to hold time, two cities at most ≈ 2000 km apart along the equator can be connected (simultaneous links to both the cities are needed in this case (see Fig. 3). Whereas if a CSAC with the ability to hold time at 1 ns precision for around 100 s is onboard, this scale doubles to around 4000 km (and hence covering the contiguous U.S.). See Figs. 6 and 8.

(iii) Satellites in higher orbits give smaller ebit rates but longer connectivity and larger network coverage areas. This means there is a nontrivial trade-off between precision and coverage areas (see Figs. 6 and 7). Our results show that for a 1 ns precision requirement, MEO satellites with smaller onboard clock stability can provide better connectivity for the

TABLE II. QCS network figures of merit for ground-station pairs in the contiguous U.S. with a constellation of ten MEO satellites (two tilted polar orbits of five satellites each). Orbit altitudes are set to 5000 km, ebit connection rate threshold \mathcal{R}_c at 200 ebits/s and hold over time τ at 100 s. Average ebit losses for uplink and downlink are reported from each ground station in decibels (this includes detector inefficiencies ≈ 6 dB). An average loss of 30 decibels converts to an ebit loss fraction of 10^{-3} . Therefore, if the entangled source rate is 10^7 ebits/s then, on average, 10 000 ebits are detected between the satellite and ground station per second when a connection is established. Figures of merit show considerable increase in the connectivity even for a modest hold over time. Also, the losses are more uniform—all cities now operate at around the same precision as against the LEO case in Table I where the losses range from 26–44 dB. Although some cities now receive lower ebit rates than the LEO case, setting the cutoff rate guarantees better than 1 ns precision.

$h = 5000$ km, $\mathcal{R}_c = 200$ ebits/s, $\tau = 100$ s				
Ground station pair (GS1/GS2)	Average uplink ebit loss(dB/dB)	Average downlink ebit loss (dB/dB)	Percent of day connected	Longest connection gap (hours)
NYC/LA	37/38	37/37	60%	4
NYC/SEA	37/38	37/38	60%	3
NYC/ATL	37/37	37/37	89%	1
LA/SEA	38/38	38/37	91%	0.8
LA/ATL	37/37	37/37	68%	3
SEA/ATL	38/37	37/36	66%	3

contiguous U.S. network, compared to LEO satellites with more stable clocks (compare Tables I and II). This also translates to an increase in the coverage area when moving from a LEO to a MEO constellation, for the same choice of onboard hardware parameters.

(iv) Optimal orientation of the orbit leads to increase in network scale (e.g., a tilted orbit at -50° angle with the Earth’s axis of rotation lets us cover the continental U.S. whereas a nontilted polar orbit fails to do so). See Fig. 11.

(v) Adding more satellites in an orbit (up to a threshold number) gives higher connected time percentages by reducing the length of short gaps between connections, and a larger number of orbits reduces the longer time gaps between satellite and ground station connections (see Figs. 5 and 10). Since intersatellite links are not considered in this paper, two ground stations can only be connected if they are in view of a common satellite. It should thus be noted that adding satellites to the constellation cannot enhance the scale of the network.

Finally, in Sec. IV C, by using static simulations, we justify the use of ebit rate thresholds as a proxy for sync precision and show the relationship between these quantities. We also study the effect of loss, dark counts, and jitter on the sync precision. We further establish that the acquisition times required to perform the sync at subnanosecond levels is around 250 ms.

An important implication of this short acquisition time is that since relativistic effects produce less than a nanosecond of relative clock drift per second between the satellite and ground station [17], they can be safely ignored for the QCS protocol if the sync requirements are at the nanosecond level.

VI. DISCUSSION AND FUTURE WORK

This paper contains a study of the feasibility and performance capabilities of a QCS protocol to distribute time across the globe using networks of satellites equipped with quantum resources. The protocol comes with the added advantage that it can sync clocks independent of ranging (i.e., knowledge of distances) and hence is more robust to trajectory inaccuracies and delay attacks, in addition to the extra layer of *quantum security* associated with the polarization state entanglement. We find that large-area networks of synchronized clocks can be established with modest resources of a handful of quantum-enabled satellites with modest equipment onboard, with expected sync precision of a few nanoseconds going up to tens of picoseconds—higher than the GPS. In particular, these satellites do not need to have intersatellite communication capabilities and

TABLE III. Static simulation results: Varying link loss with fixed acquisition time ($T_a = 250$ ms), 50 ps time-stamp resolution, no timing jitter, satellite clock frequency accuracy of 3×10^{-10} , and 1000 Hz dark count rate with 50% detection efficiency per detector. The simulation includes no loss between the photon pair source and local detectors. Successful cases are those whose simulated clock offset estimate is within 1 ns of the true value.

Link photon loss (dB)	Success rate (%)	Mean ebit rate (ebits/s)	Mean cross correlation SNR	Mean clock offset error (ps)	Mean offset error successful cases (ps)
34.0	100	995	76.8 ± 6.0	29 ± 0	Same
36.0	100	628	59.2 ± 5.4	28 ± 0	Same
38.0	100	396	44.7 ± 5.2	39 ± 0	Same
40.0	100	250	28.2 ± 4.3	48 ± 16	Same
42.0	100	158	19.6 ± 3.3	36 ± 25	Same
44.0	97	100	15.2 ± 3.4	$(0.2 \pm 1.2) \times 10^6$	43 ± 0
46.0	54	63	11.1 ± 2.1	$(2.3 \pm 7.8) \times 10^6$	33 ± 0

TABLE IV. Static simulation results: Varying link loss with fixed acquisition time ($T_a = 250$ ms), 50 ps time-stamp resolution, 100 ps detector timing jitter (FWHM), satellite clock frequency accuracy of 3×10^{-10} , and 1000 Hz dark count rate with 50% detection efficiency per detector. The simulation includes no loss between the photon pair source and local detectors. Successful cases are those whose simulated clock offset estimate is within 1 ns of the true value.

Link photon loss (dB)	Success rate (%)	Mean ebit rate (ebits/s)	Mean cross correlation SNR	Mean clock offset error (ps)	Mean offset error successful cases (ps)
34.0	100	995	23.2 ± 2.5	42 ± 42	Same
36.0	100	628	18.8 ± 2.7	42 ± 45	Same
38.0	100	396	14.5 ± 2.3	43 ± 53	Same
40.0	80	250	11.3 ± 1.9	$(0.7 \pm 5.3) \times 10^6$	47 ± 51
41.0	67	199	10.4 ± 1.6	$(0.5 \pm 10.1) \times 10^6$	25 ± 60
42.0	35	158	9.8 ± 1.3	$(1.4 \pm 9.2) \times 10^6$	22 ± 39
44.0	1	100	9.2 ± 0.7	$(3.7 \pm 13.6) \times 10^6$	145

need only to have relatively stable clocks, satellite-ground (uplink and downlink) quantum communication capabilities, and reasonable quantum hardware (entangled photon-pair sources and photodetectors). These ingredients are common to the requirements of current space missions which seek to establish quantum communication links (e.g., long-distance QKD). Hence, our clock synchronization protocol adds an extra layer of utility to quantum technologies in the space domain.

A takeaway of our analysis is that, by adding more functionality to the satellites—particularly, intersatellite quantum communication capabilities—it is plausible that major cities across the globe can share a quantum-secure, highly synchronized common time, using a modest amount of resources which could also have other functionality. The advantages of such a “clock network in the sky” do not come for free, as this is a configuration that will require more resources. At the same time, this remains a feasible concept, since the intersatellite communication occurs essentially in vacuum, involving minimum losses. The limiting factor for such configuration would still be satellite-ground station communication. In fact, if we consider that such a master clock has been created, we can use the simulation developed in this work to assess the network outcomes. In Table VII, we show these for a representative network of six cities spread across the globe. The ground stations are based in the cities Seattle (SEA), USA; New Delhi (DEL), India; London (LON), UK;

Sydney (SYD), Australia; Cape Town (CAP), South Africa; Rio Grande (RIG), Argentina. The loss figures indicate average loss for all cities (since the links are independent, all satellite-ground station links have the same average loss levels). The results are encouraging, suggesting the availability of almost continuous subnanosecond global time standard using 10×4 distribution of 40 LEO satellites. Therefore, further studies into the feasibility of such a network are germane.

A detailed study of the capabilities of such a network is an important goal of future work. A first step will be to study the sync of multiple satellites sharing an orbit. This is a relatively straightforward task: satellites do not move significantly relative to each other, and each satellite only needs to sync with the nearest neighbor to achieve global synchronization among all satellites in the orbit (robustness can be increased by interlinking to farther neighbours). Such a simple satellite configuration should be able to sync ground stations distributed across much larger areas by synchronizing each customer with the closest satellite in view. The next step will be to study the sync of satellites in different orbits, where relative velocities will need to be taken into account. Once such a master clock is established, as shown in the preliminary results, global time distribution can indeed be achieved by using a small constellation of LEO satellites.

Another interesting future work direction would be the study of security for the QCS network. Note that the quantum entanglement of photon pairs created at Alice’s and/or Bob’s

TABLE V. Static simulation results: Varying link loss with fixed acquisition time ($T_a = 250$ ms), 100 ps time-stamp resolution, 200 ps detector timing jitter (FWHM), satellite clock frequency accuracy of 3×10^{-10} , and 1000 Hz dark count rate with 50% detection efficiency per detector. The simulation includes no loss between the photon pair source and local detectors. Successful cases are those whose simulated clock offset estimate is within 1 ns of the true value.

Link photon loss (dB)	Success rate (%)	Mean ebit rate (ebits/s)	Mean cross correlation SNR	Mean clock offset error (ps)	Mean offset error successful cases (ps)
34.0	100	995	14.9 ± 1.6	39 ± 82	Same
36.0	100	628	12.2 ± 1.7	59 ± 105	Same
38.0	98	396	9.8 ± 1.3	$(0.5 \pm 3.9) \times 10^6$	43 ± 97
40.0	54	250	8.3 ± 1.1	$(0.3 \pm 1.2) \times 10^7$	52 ± 122
41.0	26	199	7.9 ± 0.8	$(0.7 \pm 18.2) \times 10^6$	47 ± 158
42.0	10	158	7.9 ± 0.6	$(0.5 \pm 2.2) \times 10^7$	14 ± 118
44.0	2	100	7.9 ± 0.5	$(0.5 \pm 2.0) \times 10^7$	128 ± 0

TABLE VI. Static simulation results: Varying acquisition time with a fixed link loss between the satellite and ground station (41 dB) and no loss for the local signal, satellite clock frequency accuracy of 3×10^{-10} , 50 ps time-stamp resolution, 100 ps detector timing jitter (FWHM), and 1000 Hz dark count rate with 50% detection efficiency per detector. The simulation includes 0 dB of loss between the photon pair source and local detectors. Successful cases are those whose simulated clock offset estimate is within 1 ns of the true value.

Acquisition time (ms)	Success rate (%)	Mean ebit rate (ebits/s)	Average total ebits	Mean cross correlation SNR	Mean clock offset error (ps)	Mean offset error successful cases (ps)
100	13	199	20	10.9 ± 1.1	$(0.6 \pm 1.4) \times 10^7$	68 ± 56
150	30	199	30	10.5 ± 1.3	$(0.2 \pm 1.2) \times 10^7$	41 ± 52
200	42	199	40	10.3 ± 1.5	$(0.2 \pm 1.0) \times 10^7$	44 ± 52
250	67	199	50	10.4 ± 1.6	$(0.5 \pm 10.0) \times 10^6$	25 ± 60
500	96	199	99	11.0 ± 1.6	$(0.4 \pm 2.5) \times 10^6$	80 ± 52

locations does not play a direct role in determining the clock offset estimate, except that the production of entangled pairs by SPDC ensures that the photons in each pair are generated within a time window typically of a few 100 fs, several orders of magnitude smaller than the timescales involved in the synchronization protocol. However, the entanglement between photon pairs plays a crucial role in increasing the security of this protocol to malicious attacks since it can be used to directly verify the detected photons used for the clock offset estimates. Violation of Bell's inequality implies that the correlations in the photon pair's polarization could not have been fully copied and therefore spoofed by an adversary. Under the assumption of channel reciprocity (i.e., that the propagation time is the same in each direction), this verification ensures the security of the estimated clock offset. This follows due to the bidirectional nature of the two-way QCS protocol since reciprocity implies that symmetric delays introduced into the channel by an adversary will have no effect on the estimated clock offset. In the case of free space optical channels through the atmosphere, only very small deviations from full reciprocity are typically incurred. For instance, between a Medium Earth Orbiting (MEO) satellite and ground station, the maximum error due to turbulence-induced nonreciprocity is predicted to be less than 10 fs [29,30]. Partial reciprocity and other nonidealities of practical implementations would likely place a limit on the achievable *secure* accuracy of the clock synchronization protocol. Thus, an analysis of the system requirements for using the detected entangled photons to warrant a specified level of security for

the distributed time information is also the focus of future work.

The present paper also contains several limitations. We have used the quantum communication rates as a proxy for sync performance and considered the effects of a possible constant relative velocity between the ground stations and satellites. In a real situation, however, these relative velocities are not constant and, as discussed in Secs. II A and IV, to quantify the effects they have on the sync precision, one needs a real-time calculation of correlation functions. Although such calculation goes beyond the scope of this paper, our analysis shows that the time needed for a ground station to synchronize with a satellite (what we have called the acquisition time) is sufficiently short for the relative velocities to be well approximated by a constant value. Although the concrete value of the acquisition time depends on the losses and noise levels (other hardware parameters remaining fixed), our calculations show that typical values are not more than a few hundred milliseconds. This interval is short enough for the relative velocity between satellite and ground stations to remain constant.

Similarly, we have not included the impact of relativistic effect in this paper. One could have the impression that, since relativist effects play an important role in other satellite-based synchronization systems and, in particular, for the GPS, they should play an even more important role in the protocol we study in this paper, since it aims at a better sync precision. Again, the key observation is that the acquisition time required to establish synchronization is estimated to be not more than a fraction of a second, and such an interval is not long

TABLE VII. QCS network figures of merit (FOM) for a global QCS network. The representative ground stations are based in the cities Seattle, USA; New Delhi, India; London, UK; Sydney, Australia; Cape Town, South Africa and Rio Grande, Argentina. Constellation configurations at 500 and 1000 km orbit altitudes. Configurations are shown as $n \times o$, where n represents the number of satellites in a particular orbit while o represents the number of distinct orbits, e.g., 10×4 should be interpreted as a total of 40 satellites distributed in four polar orbits of ten satellites each. The rate cutoff is set at $\mathcal{R}_c = 100$ ebits/s. Note that the entries in the table written as ranges indicate that the quantities vary across the cities within that range. For example, 60–80% connection fraction range in the 10×4 configuration indicates that the connection fraction varies from the lowest of 60% of the day for New Delhi to the highest of 80% of the day for Rio Grande.

Altitude	Network FOM	10×1	5×2	10×4	5×8
500 km	Average uplink/downlink loss (dB/dB)	29/25	29/25	29/25	27/23
	Connection time (% of the day)	15–22	15–20	60–80	43–44
	Longest connection gap (hours)	8.5–9.5	3.0–3.5	0.1–0.7	0.18–0.19
1000 km	Avg. uplink/downlink loss (dB/dB)	30/29	31/29	29/27	29/27
	Connection time (% of the day)	27–41	30–45	98–100	65–69
	Longest connection gap (hours)	6.5–8.5	1.0–2.5	0.02–0.03	0.12–0.14

enough for relativistic effects to build up significantly [17]. Conversely, if synchronization can be established fast enough in a realistic setting, the QCS network could be thought of as a precise measurement device for relativistic effects around the Earth. Many of the leading and higher order relativistic effects could be in the range of measurement through a near-term implementation of the ideas proposed here. This, in turn, would also provide a way to measure the effects of weak gravity on quantum systems, complementing dedicated studies [44–49]. These and other extensions—such as the use of realistic orbits, aspects of the extra security layer added by the entanglement in polarization of photons, etc.—will be the focus of future work.

ACKNOWLEDGMENTS

This work was partially supported by the U.S. SBIR/STTR program under Air Force Research Laboratory Contract No. FA9453-20-P-0100 and NASA Contract No. 80NSSC20C0395. J.E.T. acknowledges additional support from Xairos Systems, Inc. I.A. is supported by NSF Grant No. PHY-2110273, from Xairos Systems Inc., and from the Hearne Institute for Theoretical Physics at Louisiana State University.

APPENDIX A: LOSS MODELS USED IN THE SIMULATION

Here we describe the loss model used in our simulations of the uplink and downlink closely following Khatri *et al.* [7]. We consider both the free space links as pure bosonic loss channels (erasure channel). This is done both for simplicity and also motivated by the fact that the QCS protocol only uses the tight time correlations between the entangled state photons and not their polarization correlations. For a more detailed and exact noise model, see Vasylyev *et al.* [50]. The change in the quantum state of the photons as they traverse through the channels is thus not very important for the QCS protocol, only whether or not they arrive at the detectors at the other end is relevant. The state of each of the photons as they travel through the channel evolves as follows:

$$\rho \rightarrow \eta\rho + (1 - \eta)|0\rangle\langle 0|, \quad (\text{A1})$$

where η is the uplink or downlink transmissivity, i.e., the probability with which a photon gets transmitted through the channel. $|0\rangle$ is the vacuum state (no photon). The transmissivity η has three factors:

(i) Free space transmittance: This includes effects of beam broadening and finite apertures of the transmitting and receiving telescopes. The free space transmittance thus follows an inverse square fall off law with the link distance and is given by

$$\eta_{\text{fs}}(L) = 1 - \exp\left(-\frac{2R^2}{w(L)^2}\right), \quad (\text{A2})$$

where R is the receiving telescope's radius and $w(L)$ is the beam waist after traversing the link distance L . The latter is given by

$$w(L) := w_0\sqrt{1 + \left(\frac{L}{L_R}\right)^2} \quad (\text{A3})$$

and the Rayleigh range $L_R := \pi w_0^2 \lambda^{-1}$. λ is the source wavelength and w_0 is the initial beam-waist radius. $w_0 = 0.8r$, where r is the transmitting telescope's radius and we use a 80% fill fraction. The above relation holds under the approximation of the beam as a zeroth order Gaussian spatial mode.

(ii) Atmospheric transmittance: Here we assume the atmosphere to be a homogeneous absorptive medium following the Beer-Lambert's Law (transmittance falls exponentially with increasing distance that is traveled through the medium). Thus, the atmospheric transmittance is given as

$$\eta_{\text{atm}}(L, h) = \begin{cases} (\eta_{\text{atm}}^{\text{zen}})^{\sec \zeta}, & \text{if } -\frac{\pi}{2} < \zeta < \frac{\pi}{2} \\ 0, & \text{if } |\zeta| \geq \frac{\pi}{2}, \end{cases} \quad (\text{A4})$$

$\eta_{\text{atm}}^{\text{zen}}$ is the atmospheric transmittance at zenith ($\zeta = 0$) and the zenith angle ζ for circular orbits is given by

$$\cos \zeta = \frac{h}{L} - \frac{1}{2} \frac{L^2 - h^2}{R_E L}, \quad (\text{A5})$$

where R_E is the radius of Earth.

(iii) Detector inefficiencies: κ_{sat} and κ_{grd} are efficiencies of the detectors at the satellite and ground station, respectively.

Thus the total efficiency of the channel (uplink or downlink) is given by $\eta = \eta_{\text{atm}} \eta_{\text{fs}} \kappa_{\text{sat}} \kappa_{\text{grd}}$.

APPENDIX B: EBIT RATES AS A PROXY FOR SYNC PRECISION

Throughout this paper, we have used ebit rates as a proxy for sync precision. The justification for this assumption was also provided through static Monte Carlo simulations of the cross-correlation function in Sec. IV C. This can be further justified by looking at the SNR of the cross-correlation function peaks which are defined in Sec. II. The SNR can be calculated by simple physical arguments about the photon counts at various detectors (also see Ref. [1] for a similar analysis). Assume the protocol is performed within an acquisition time t_a that is small enough to consider constant channel transmissivity η . The noise in the cross-correlation function is produced by three different sources of spurious correlations: (i) photons whose partner (from the ebit) has been lost in the channel, (ii) the background noise at ground station and satellite receiving telescopes, and (iii) dark counts at all detectors. Therefore, the total number of spurious time-stamp correlations is

$$N_{\text{sp}} = (\mathcal{R}^2 \eta t_a^2 + \mathcal{R} \mathcal{R}_{\text{bkg}} t_a^2 + \mathcal{R} \mathcal{R}_{\text{dc}} t_a^2), \quad (\text{B1})$$

where \mathcal{R}_{bkg} and \mathcal{R}_{dc} are the background noise and dark count rates at the receiving telescopes, respectively (for simplicity, assuming them to be the same at the satellite and ground station). The noise in the cross correlations can be calculated considering that all these photons have uniformly random time of birth correlations and therefore are uniformly divided among all the time bins of the cross-correlation function. The number of time bins is given by $n = t_a/t_{\text{bin}}$, where t_{bin} is the precision at which we want to run the protocol. The mean height of these spurious correlations is thus given by

$$C_{\text{sp}} = \frac{N_{\text{sp}}}{n}. \quad (\text{B2})$$

The total number of entangled photon pairs generated in time interval t_a form the signal peak. The height of this peak above the noise floor created by spurious correlations is given by (the noise floor height also adds to the signal)

$$C_{\text{sg}} = \frac{\mathcal{R}\eta t_a}{n}, \quad (\text{B3})$$

where \mathcal{R} is the ebit rate for the SPDC source. The SNR of the cross-correlation peak is thus given by

$$S := \frac{C_{\text{sg}}}{\sqrt{C_{\text{sp}}}} = \sqrt{\frac{\eta t_{\text{bin}}}{t_a \left(1 + \frac{\mathcal{R}_{\text{bkg}} + \mathcal{R}_{\text{dc}}}{\mathcal{R}\eta}\right)}}. \quad (\text{B4})$$

The probability ϵ that an untrue time offset value gives the highest peak with SNR equal to S is given by Ref. [1],

$$\epsilon = \frac{n}{2} \left(1 - \operatorname{erf}\left(\frac{S}{\sqrt{2}}\right)\right), \quad (\text{B5})$$

Therefore, inverting the relation in equation (B4), we can find the precision t_{bin} given a required success probability $1 - \epsilon$ and the associated SNR given by Eq. (B5). This precision is given as

$$t_{\text{bin}} = (S)^2 \frac{t_a}{\eta} \left(1 + \frac{\mathcal{R}_{\text{bkg}} + \mathcal{R}_{\text{dc}}}{\mathcal{R}\eta}\right). \quad (\text{B6})$$

It is clear from Eq. (B6) that the sync precision increases when the source rate \mathcal{R} or the channel transmissivity η increase. This justifies the choice of ebit rates received at the ground station or the satellite, which is equal to $\mathcal{R}\eta$, as a proxy for sync precision. One of the limitations of this proxy analysis is the assumption that the acquisition time is fixed. Since the acquisition time is an experimental choice, this could very well be the case but, nonetheless, the total available acquisition time depends on dynamic variables such as visibility of the satellite with respect to the ground station, the relative velocity between them, and the error in its estimated value.

APPENDIX C: DETAILS OF THE DYNAMIC SIMULATION CODE

In this Appendix, we briefly list some computational aspects of the dynamic simulation of the QCS network. This closely follows the simulations developed in Khatri *et al.* [7], which have been adapted here for the QCS protocol. Their key difference being moving from a double downlink scenario (entanglement distribution between ground stations) to an uplink-downlink scenario for the QCS protocol.

(i) The coordinates of the satellites and ground stations are stored in custom data structures in Python referred to as dictionaries. A dictionary is similar to a structured table with multiple keys. In our case, the two keys are satellite labels, viz., the orbit number and the satellite number within the orbit $[i, j]$. The satellite coordinates $r_{i,j}$ are stored as $S[i][j] = r_{i,j}$. Each label $[i]$ has an additional index [“axis”], storing the axis of the i th orbit. Ground stations only have one key indicating their assigned city number.

(ii) The evolution is done in a time discrete manner. We choose $dt = 1$ s for all our simulations. A time-efficient

implementation of dynamics for multiple cities and satellites requires parallel computing tools. We use the *Joblib* library in Python to perform time evolution computations in parallel. Each job finds the coordinates at time t , starting always from $t = 0$, such that all jobs remain independent and can be performed in parallel instead of a sequential evolution. This is done by multiplying the coordinate vector r_{ij} with an appropriate rotation matrix $R_i(t)$, where i refers to the orbit number and t is the evolution time step. Using 50 cores (parallel jobs) reduces the run time by at least two orders of magnitude, and hence allows us to simulate two days of time evolution for up to 100 satellites and six to ten cities easily in computation time of a few hours.

(iii) Since generating the time evolution data is the most time-consuming step of the simulation, we do so once for a given configuration of satellites and ground stations. Also, when coordinates are evolved, we find the distances and inclination angles between cities and ground stations. Using the definitions of transmissivity η in Appendix A and the visibility condition, losses for all the uplinks and downlinks are calculated. The data is also stored in the form of a dictionary which has the following form: `Data[t][“groundstation”][label][“inrange”] = ((k, l), d, η_u , η_d , t)`. The ground station key indicates that the data is with respect to a particular ground station. The label key is the ground-station index. The “inrange” key indicates that the data is stored only for satellites that are in range of the ground station. A satellite is considered in range (visible) only if it is above the horizon and if the rate received is $\geq \mathcal{R}_c$. (k, l) are the satellite indices, d is the link length (distance between ground station and satellite), and η_u and η_d are the calculated uplink and downlink transmissivity values for the ([label], (k, l)) ground station–satellite pair. All the data of the positions and ebit rates, etc. (at all times) are then stored in a file using the *Pickle* package in Python, which is an efficient file handling system for structured data like dictionaries, allowing its writing and reading with single line commands.

(iv) Finally, to extract the relevant figures of merit from the time evolution data, given a cutoff rate \mathcal{R}_c and hold-over time τ , we write the following functions:

(1) Avg ebit rate (uplinks and downlinks): When calculating the ebit rate available at ground station A for synchronizing it with another ground station B, we make a separate dictionary with all the satellites that are in range of both A and B within the holdover time τ . This dictionary stores the respective uplink and downlink rates. A maximization is then done over the rates from all the in range satellites and over the entire hold over window centered around a given time t . These maximized rates constitute the *sync traces* defined in Sec. IV A 1. The average is then calculated using these maximized rates.

(2) Connected fraction: Once the ebit rates as a function of time (sync traces) are known, it is easy to find the total time for which the connection was established (sync trace was nonzero, since this already includes the effect of cutoff rates and hold over times).

(3) Longest disconnected times: Similar to the connection fraction, this figure of merit can also be calculated easily from the sync traces.

- [1] C. Ho, A. Lamas-Linares, and C. Kurtsiefer, *New J. Phys.* **11**, 045011 (2009).
- [2] A. Lamas-Linares and J. Troupe, SPIE 10547, *Adv. Photonics Quantum Comput. Memory Commun.* XI 10547 (2018).
- [3] J. Lee, L. Shen, A. Cerè, J. Troupe, A. Lamas-Linares, and C. Kurtsiefer, *Appl. Phys. Lett.* **114**, 101102 (2019).
- [4] C. Spiess, S. Töpfer, S. Sharma, A. Kri, M. C. Ponce, U. Chandrashekhara, N. L. Döll, D. Rieländer, and F. Steinlechner, Clock synchronization with correlated photons [arXiv:2108.13466](https://arxiv.org/abs/2108.13466).
- [5] R. Lafler and R. N. Lanning, Quantum time transfer for freespace quantum networking [arXiv:2211.00737](https://arxiv.org/abs/2211.00737).
- [6] X. Xiang, B. Shi, R. Quan, Y. Liu, Z. Xia, H. Hong, T. Liu, J. Wu, J. Qiang, J. Jia, S. Zhang, and R. Dong, Quantum two-way time transfer over a hybrid free-space and fiber link [arXiv:2212.01741](https://arxiv.org/abs/2212.01741).
- [7] S. Khatri, A. J. Brady, R. A. Desporte, M. P. Bart, and J. P. Dowling, *npj Quantum Inf.* **7**, 4 (2021).
- [8] Microchip, SA65 CSAC Datasheet, <https://www.microchip.com/en-us/product/CSAC-SA45S> (accessed Dec. 26, 2021).
- [9] W. F. McGrew, X. Zhang, R. J. Fasano, S. A. Schäffer, K. Beloy, D. Nicolodi, R. C. Brown, N. Hinkley, G. Milani, M. Schioppa, T. H. Yoon, and A. D. Ludlow, *Nature (London)* **564**, 87 (2018).
- [10] E. Oelker, R. Hutson, C. Kennedy, L. Sonderhouse, T. Bothwell, A. Goban, D. Kedar, C. Sanner, J. Robinson, G. Marti, D. Matei, T. Legero, M. Giunta, R. Holzwarth, F. Riehle, U. Sterr, and J. Ye, *Nat. Photonics* **13**, 714 (2019).
- [11] P. Delva, F. Meynadier, C. Le Poncin-Lafitte, P. Laurent, and P. Wolf, Time and frequency transfer with a microwave link in the ACES/PHARAO mission, *2012 European Frequency and Time Forum, Gothenburg, Sweden* (IEEE, 2012), pp. 28–35.
- [12] J.-D. Deschênes, L. C. Sinclair, F. R. Giorgetta, W. C. Swann, E. Baumann, H. Bergeron, M. Cermak, I. Coddington, and N. R. Newbury, *Phys. Rev. X* **6**, 021016 (2016).
- [13] H. Bergeron, L. C. Sinclair, W. C. Swann, I. Khader, K. C. Cossel, M. Cermak, J.-D. Deschênes, and N. R. Newbury, *Nat. Commun.* **10**, 1819 (2019).
- [14] S. Dolinar, K. M. Birnbaum, B. I. Erkmen, and B. Moision, *2011 International Conference on Space Optical Systems and Applications (ICSOS)* (IEEE, 2011), pp. 269–278.
- [15] IEEE, IEEE Standard for a precision clock synchronization protocol for networked measurement and control systems, IEC 61588:2009(E) (2009).
- [16] Wrin1588 wiki projects / white rabbit standardization, <https://ohwr.org/projects/wr-std/wiki/wrin1588>.
- [17] S. Y. Zhu and E. Groten, *GPS-Techniques Applied to Geodesy and Surveying*, edited by E. Groten and R. Strauß, Lecture Notes in Earth Sciences Vol. 19 (Springer-Verlag, Heidelberg, 1988), pp. 41–46.
- [18] A. O'Connor, M. Gallaher, K. Clark-Sutton, D. Lapidus, Z. Oliver, T. Scott, D. Wood, M. Gonzalez, E. Brown, and J. Fletcher, Economic benefits of the global positioning system (GPS), report sponsored by the National Institute of Standards and Technology, 2019.
- [19] I. F. Akyildiz, A. Kak, and S. Nie, *IEEE Access* **8**, 133995 (2020).
- [20] S. Bush, W. Challener, and G. Mantelet, *AVS Quantum Sci.* **3**, 030501 (2021).
- [21] P. Rochat, F. Droz, Q. Wang, and S. Froidevau, Atomic clocks and timing systems in global navigation satellite systems, Proceedings of European Navigation Conference (2021).
- [22] R. Jozsa, D. S. Abrams, J. P. Dowling, and C. P. Williams, *Phys. Rev. Lett.* **85**, 2010 (2000).
- [23] V. Giovannetti, S. Lloyd, and L. Maccone, *Nature (London)* **412**, 417 (2001).
- [24] V. Giovannetti, S. Lloyd, L. Maccone, J. H. Shapiro, and F. N. C. Wong, *Phys. Rev. A* **70**, 043808 (2004).
- [25] A. Valencia, G. Scarcelli, and Y. Shih, *Appl. Phys. Lett.* **85**, 2655 (2004).
- [26] U. Yurtsever and J. P. Dowling, *Phys. Rev. A* **65**, 052317 (2002).
- [27] E. O. Ilo-Okeke, L. Tessler, J. P. Dowling, and T. Byrnes, *npj Quantum Inf.* **4**, 40 (2018).
- [28] D. C. Burnham and D. L. Weinberg, *Phys. Rev. Lett.* **25**, 84 (1970).
- [29] A. Belmonte, M. Taylor, L. Holberg, and J. Kahn, *Opt. Express* **25**, 15676 (2017).
- [30] M. T. Taylor, A. Belmonte, L. Hollberg, and J. M. Kahn, *Phys. Rev. A* **101**, 033843 (2020).
- [31] J. Yin, Y.-H. Li, S.-K. Liao, M. Yang, Y. Cao, L. Zhang, J.-G. Ren, W.-Q. Cai, W.-Y. Liu, S.-L. Li, R. Shu, Y.-M. Huang, L. Deng, L. Li, Q. Zhang, N.-L. Liu, Y.-A. Chen, C.-Y. Lu, X.-B. Wang, F. Xu *et al.*, *Nature (London)* **582**, 501 (2020).
- [32] J. S. Sidhu, S. K. Joshi, M. Gündogan, T. Brougham, D. Lowndes, L. Mazzarella, M. Krutzik, S. Mohapatra, D. Dequal, G. Vallone, P. Villoresi, A. Ling, T. Jennewein, M. Mohageg, J. Rarity, I. F. amd Stefano Pirandola, and D. K. L. Oi, *IET Quantum Commun.* **1**, 1 (2021).
- [33] S. Wang, *Light Sci. Appl.* **11**, 301 (2022).
- [34] G.-J. Fan-Yuan, F.-Y. Lu, S. Wang, Z.-Q. Yin, D.-Y. He, Z. Zhou, J. Teng, W. Chen, G.-C. Guo, and Z.-F. Han, *Photonics Res.* **9**, 1881 (2021).
- [35] G.-J. Fan-Yuan, F.-Y. Lu, S. Wang, Z.-Q. Yin, D.-Y. He, W. Chen, Z. Zhou, Z.-H. Wang, J. Teng, G.-C. Guo, and Z.-F. Han, *Optica* **9**, 812 (2022).
- [36] J.-G. Ren, P. Xu, H.-L. Yong, L. Zhang, S.-K. Liao, J. Yin, W.-Y. Liu, W.-Q. Cai, M. Yang, L. Li, K.-X. Yang, X. Han, Y.-Q. Yao, J. Li, H.-Y. Wu, S. Wan, L. Liu, D.-Q. Liu, Y.-W. Kuang, Z.-P. He *et al.*, *Nature (London)* **549**, 70 (2017).
- [37] H. Dai, Q. Shen, C.-Z. Wang, S.-L. Li, W.-Y. Liu, W.-Q. Cai, S.-K. Liao, J.-G. Ren, J. Yin, Y.-A. Chen, Q. Zhang, F. Xu, C.-Z. Peng, and J.-W. Pan, *Nat. Phys.* **16**, 848 (2020).
- [38] A. Villar, A. Lohrmann, X. Bai, T. Vergoossen, R. Bedington, C. Perumangatt, H. Y. Lim, T. Islam, A. Reezwana, Z. Tang, R. Chandrasekhara, S. Sachidananda, K. Durak, C. F. Wildfeuer, D. Griffin, D. K. L. Oi, and A. Ling, *Optica* **7**, 734 (2020).
- [39] PlaneWave Instruments, Corrected Dall-Kirkham (CDK) Telescope Specifications, <https://planewave.com/cdk-telescopes> (accessed Dec. 26 2021).
- [40] California-Polytechnic-State University, CubeSat Design Specification Revision 14, <https://www.cubesat.org/cds-announcement> (accessed Dec. 26, 2021).
- [41] D. K. Oi, A. Ling, G. Vallone, P. Villoresi, S. Greenland, E. Kerr, M. Macdonald, H. Weinfurter, H. Kuiper, E. Charbon, and R. Ursin, *EPJ Quantum Technol.* **4**, 6 (2017).
- [42] M. Lombardi, The accuracy and stability of quartz watches, <https://tf.nist.gov/general/pdf/2276.pdf>.

- [43] J. S. Sidhu, T. Brougham, D. McArthur, R. G. Pousa, and D. K. L. Oi, [npj Quantum Inf.](#) **8**, 18 (2022).
- [44] D. Rideout, T. Jennewein, G. Amelino-Camelia, T. F. Demarie, B. L. Higgins, A. Kempf, A. Kent, R. Laflamme, X. Ma, R. B. Mann, E. Martin-Martinez, N. C. Menicucci, J. Moffat, C. Simon, R. Sorkin, L. Smolin, and D. R. Terno, [Class. Quantum Grav.](#) **29**, 224011 (2012).
- [45] A. J. Brady and S. Haldar, [Phys. Rev. Res.](#) **3**, 023024 (2021).
- [46] M. Rivera-Tapia, A. Delgado, and G. Rubilar, [Classical Quantum Gravity](#) **37**, 195001 (2020).
- [47] D. R. Terno, F. Vedovato, M. Schiavon, A. R. H. Smith, P. Magnani, G. Vallone, and P. Villoresi, [arXiv:1811.04835](#).
- [48] H. Abele and H. Leeb, [New J. Phys.](#) **14**, 055010 (2012).
- [49] G. M. Tino, A. Bassi, G. Bianco, K. Bongs, P. Bouyer, L. Cacciapuoti, S. Capozziello, X. Chen, M. L. Chiofalo, A. Derevianko, W. Ertmer, N. Gaaloul, P. Gill, P. W. Graham, J. M. Hogan, L. Iess, M. A. Kasevich, H. Katori, C. Klempt, X. Lu *et al.*, [Eur. Phys. J. D](#) **73**, 228 (2019).
- [50] D. Vasylyev, W. Vogel, and F. Moll, [Phys. Rev. A](#) **99**, 053830 (2019).